

**Effects of common mutations in the SARS-CoV-2 Spike RBD and its
ligand the human ACE2 receptor on binding affinity and kinetics**

Michael I. Barton¹, Stuart MacGowan², Mikhail Kutuzov¹, Omer Dushek¹, Geoffrey J.
Barton^{2*}, and P. Anton van der Merwe^{1*}

¹Sir William Dunn School of Pathology, University of Oxford, Oxford, OX1 3RE, UK

²School of Life Sciences, University of Dundee, Dow Street, Dundee, DD1 5EH, UK

*Corresponding authors: g.j.barton@dundee.ac.uk; anton.vandermerwe@path.ox.ac.uk.

13

14 **Abstract**

15 The interaction between the SARS-CoV-2 virus Spike protein receptor binding domain (RBD)
16 and the ACE2 cell surface protein is required for viral infection of cells. Mutations in the RBD
17 are present in SARS-CoV-2 variants of concern that have emerged independently worldwide.
18 For example, the B.1.1.7 lineage has a mutation (N501Y) in its Spike RBD that enhances
19 binding to ACE2. There are also ACE2 alleles in humans with mutations in the RBD binding
20 site. Here we perform a detailed affinity and kinetics analysis of the effect of five common
21 RBD mutations (K417N, K417T, N501Y, E484K and S477N) and two common ACE2 mutations
22 (S19P and K26R) on the RBD/ACE2 interaction. We analysed the effects of individual RBD
23 mutations, and combinations found in new SARS-CoV-2 Alpha (B.1.1.7), Beta (B.1.351) and
24 Gamma (P1) variants. Most of these mutations increased the affinity of the RBD/ACE2
25 interaction. The exceptions were mutations K417N/T, which decreased the affinity. Taken
26 together with other studies, our results suggest that the N501Y and S477N mutations
27 enhance transmission primarily by enhancing binding, the K417N/T mutations facilitate
28 immune escape, and the E484K mutation enhances binding and immune escape.

29

Introduction

Since its identification in 2019, a coronavirus able to induce a severe acute respiratory syndrome in humans, SARS-CoV-2, has resulted in arguably the most severe infectious disease pandemic in 100 years. To date more than 135 million people have been infected, resulting in the deaths from the resulting disease, COVID-19, of more than 3 million people (“WHO Coronavirus (COVID-19) Dashboard,” 2021), and measures introduced to control spread have had harmful social and economic impacts. Fortunately, effective vaccines have been developed, and a global vaccination programme is underway (Mahase, 2021). New SARS-CoV-2 variants of concern are emerging that are making containment of the pandemic more difficult, perhaps by increasing transmissibility of the virus (Davies and Edmunds, 2021; Korber et al., 2020; Volz et al., 2021a, 2021b; Washington et al., 2021) and/or its resistance to protective immunity induced by previous infection or vaccines (Darby and Hiscox, 2021; Dejnirattisai et al., 2021; Garcia-Beltran et al., 2021; Madhi et al., 2021a, 2021b; Mahase, 2021). (Volz et al., 2021a, 2021b)

The SARS-CoV-2 virus enters cells following an interaction between the Spike (S) protein on its surface with angiotensin-converting enzyme 2 (ACE2) on cell surfaces (V'kovski et al., 2021). The receptor-binding domain (RBD) of the Spike protein binds the membrane-distal portion of the ACE2 protein. The S protein forms a homotrimer, which is cleaved shortly after synthesis into two fragments that remain associated non-covalently: S1, which contains the RBD, and S2, which mediates membrane fusion following the binding of Spike to ACE2 (V'kovski et al., 2021). During the pandemic mutations have appeared in the Spike protein that may increase transmissibility (Davies and Edmunds, 2021; Korber et al., 2020; Richard et al., 2021; Volz et al., 2021a, 2021b; Washington et al., 2021). One that emerged early in Europe, D614G, and quickly became dominant globally (Korber et al., 2020), increases the density of intact Spike trimer on the virus surface by preventing premature dissociation of S1 from S2 following cleavage (Zhang et al., 2021, 2020). A later mutation, N501Y, which has appeared in multiple lineages, lies within the RBD, and increases its affinity for ACE2 (Starr et al., 2020; Supasa et al., 2021). These findings suggest that mutations that directly or indirectly enhance Spike binding to ACE2 may increase transmissibility.

Prior infection by SARS-CoV-2 and current vaccines induce antibody responses to the Spike protein, and most neutralizing antibodies appear to bind to the Spike RBD (Garcia-Beltran et al., 2021; Greaney et al., 2021a; Rogers et al., 2020). Some variants of concern have mutations in their RBD that confer resistance to neutralizing antibodies (Darby and Hiscox, 2021; Dejnirattisai et al., 2021; Garcia-Beltran et al., 2021; Madhi et al., 2021a, 2021b; Mahase, 2021). What is less clear is the precise effect of these mutations on the affinity and kinetics of the binding of RBD to ACE2. Previous studies of the interaction between the Spike RBD and ACE2 have produced a wide range of affinity and kinetic estimates under conditions (e.g. temperature) that are not always well defined (Lei et al., 2020; Shang et al., 2020; Supasa et al., 2021; Wrapp et al., 2020; Zhang et al., 2021, 2020). Precise information is needed to assess the extent to which RBD mutations have been selected because they enhance ACE2 binding or facilitate immune evasion.

In this study we undertook a detailed affinity and kinetic analysis of the interaction between Spike RBD and ACE2 at a physiological temperature (37°C), taking care to avoid common pitfalls. We used this optimized approach to analyse the effect of important common mutations identified in variants of RBD and ACE2. Both mutations of ACE2 (S19P, K26R) and most of the mutations of RBD (N501Y, E484K, and S477N) enhanced the interaction, with one RBD mutation (N501Y) increasing the affinity by ~10 fold. Increased binding was the result of decreases in dissociation rate constants (N501Y, S477N) and/or increases in association rate constants (N501Y, E484K). Although the K417N/T mutations found in the South African (B.1.351) and Brazilian (P.1) variants both decreased the affinity, the affinity-enhancing N501Y and E484K mutations that are also present in both variants confer a net ~4 fold increase in the affinity of their RBDs for ACE2.

Results

Selection of variants

The focus of this study was to analyse common and therefore important variants of RBD and ACE2. Henceforth we will refer to the common ACE2 allele and RBD of the original SARS-CoV-2 strain sequenced in Wuhan as wild type (WT). We chose mutations of RBD within the ACE2 binding site that have appeared independently in multiple SARS-CoV-2 lineages/clades (Figure 1 and Figure 1-figure supplement 1) (Hodcroft, 2021; Rambaut et al., 2020),

suggesting that they confer a selective advantage, rather than emerged by chance, such as through a founder effect. The N501Y mutation has appeared in the Alpha (B.1.1.7; 20I/501Y.V1), Beta (B.1.351; 20H/501Y.V2), and Gamma (P.1; 20J/501Y.V3) variants, which were first identified in the UK, South Africa and Brazil, respectively. The E484K mutation is present in the Beta and Gamma variants and has appeared independently in many other lineages, including Zeta (P.2; 20B/S.484K), B.1.1.318, Eta (B.1.525; 20A/S:484K) and Iota (B.1.526; 20C/S.484K). E484K has also appeared in VOC-202102-02, a subset of the Alpha variant identified in the UK ("SARS-CoV-2 Variants of concern and variants under investigation - GOV.UK," 2021). The S477N mutation became dominant for periods in Australia (clade 20F) and parts of Europe (20A.EU2), and then appeared in New York in the Iota or B.1.526 lineage (H. Zhou et al., 2021). Mutations of K417 have appeared independently in the Beta and Gamma variants. Interestingly, N501Y, E484K and S477N were the main mutations that appeared following random RBD mutagenesis and in vitro selection of mutants with enhanced ACE2 binding (Zahradník et al., 2021).

We selected for analysis the two most common mutations of ACE2 within the RBD binding site, K26R and S19P (Figure 1C). They are present in 0.4% and 0.03%, respectively, of all samples in the gnomAD database (Karczewski et al., 2020), while other ACE2 mutations in the RBD binding site are much less frequent (<0.004%) (MacGowan et al., 2021). K26R is observed in all the major gnomAD populations but is most common in Ashkenazi Jews (1%), and (non-Finnish) north-western Europeans (0.6%). It is less common in Africans/African-Americans and South Asians (0.1%) and rare in Finnish (0.05%) and East-Asian (0.001%) populations. The S19P mutant is almost exclusively found in Africans/African-Americans (0.3%).

Measurement of affinity and kinetics

To measure the effects of these mutations on the affinity and kinetics of the RBD/ACE2 interaction we used surface plasmon resonance (SPR), which allows very accurate measurements, provided that common pitfalls are avoided, particularly protein aggregation, mass-transport limitations and rebinding (van der Merwe and Barclay, 1996; Myszk, 1997). Monomeric, soluble forms of the ectodomain of ACE2 and the Spike RBD were expressed in human cells, to retain native glycosylation, and purified (Figure 2-figure supplement 1). ACE2 was captured onto the sensor surface via a carboxy-terminal biotin and RBD injected

over ACE2 at different concentrations (Figure 2A). Excellent fits of 1:1 Langmuir binding model to the data yielded an association rate constant (k_{on}) of $0.9 \pm 0.05 \mu\text{M}^{-1}\text{s}^{-1}$ and a dissociation rate constant (k_{off}) of $0.067 \pm 0.0011 \text{ s}^{-1}$ (mean \pm SD, $n=6$, Table 1). These rate constants are up to 25 fold faster than previously reported for the same interaction (Lei et al., 2020; Shang et al., 2020; Supasa et al., 2021; Wrapp et al., 2020; Zhang et al., 2021). However, previous experiments were conducted at unphysiologically low temperatures (i.e. below 37°C) and under conditions in which mass-transport limitations and rebinding are highly likely (see Discussion). These factors, and the presence of protein aggregates (van der Merwe and Barclay, 1996), would all lower the measured rate constants. In contrast, our measurements were conducted at 37°C and under conditions in which mass-transfer limitation and rebinding were excluded. The latter is demonstrated by the fact that measured k_{on} and k_{off} rates approached maximal values at the low level of ACE2 immobilization ($\sim 50 \text{ RU}$) used in our experiments (Figure 2B and C). The excellent fit of the 1:1 binding model to our data excludes an effect of protein aggregates, which yield complex kinetics. The calculated dissociation constant (K_D) was $74 \pm 4 \text{ nM}$ (mean \pm SD, $n=6$, Table 1). We also measured K_D by equilibrium binding (Figure 2D), which avoids any artefacts induced by mass transfer limitations and rebinding. This K_D was very similar to the value calculated from kinetic data [$63 \pm 7.7 \text{ nM}$ (mean \pm SD, $n = 24$, Table 1)], and did not vary with immobilization level (Figure 2E), further validating our kinetic measurements. These affinity values are within the wide range reported in previous studies, which varied from K_D 6 to 133 nM (Laffebert et al., 2021; Lei et al., 2020; Liu et al., 2021; Shang et al., 2020; Supasa et al., 2021; Wrapp et al., 2020; Zhang et al., 2021).

The effect of RBD mutations

We next evaluated the effect of RBD mutations on the affinity and kinetics of binding to ACE2 (Figure 3 and Table 1). Example sensorgrams are shown of mutations that increased (N501Y, Figure 3A) or decreased (K417N, Figure 3B) the binding affinity, while the key results from all mutants are summarized in Figure 3C. The single mutations S477N, E484K and N501Y all enhanced binding. The N501Y mutation had the biggest effect, increasing the affinity ~ 10 fold to $K_D \sim 7 \text{ nM}$, by increasing the k_{on} ~ 1.8 fold and decreasing the k_{off} by ~ 7 -fold. The S477N and E484K mutations increased the affinity more modestly (~ 1.5 -fold), by decreasing the k_{off} (S477N) or increasing the k_{on} (E484K). The K417T and K417N mutations

decreased the affinity ~ 2 and ~ 4 fold, respectively, mainly by decreasing the k_{on} but also by increasing the k_{off} . Affinity-altering mutations in binding sites mainly affect the k_{off} (Agius et al., 2013) and have more modest effects on the k_{on} . Changes in electrostatic interactions can dramatically affect the k_{on} (Schreiber and Fersht, 1996), and are a plausible explanation for the effects of the mutations K417T, K417N and E484K on k_{on} . K417 forms a salt bridge with D30 on ACE2 (Lan et al., 2020), while E484 is ~ 9 Å from E75 on ACE2 (Lan et al., 2020). Thus, the mutations K417N/T and E484K would decrease and increase, respectively, long-range electrostatic forces that may accelerate association (Schreiber and Fersht, 1996).

We also examined the effect on ACE2 binding of combinations of RBD mutations, including combinations present in VOC-202102-02, a subset of the Alpha lineage (N501Y) with the E484K mutation ("SARS-CoV-2 Variants of concern and variants under investigation - GOV.UK," 2021), and the Beta and Gamma variants (Figure 3C, Table 1). In the case of VOC-202102-02, the addition of the E484K mutation to N501Y further increased the affinity, to ~ 15 fold higher than WT RBD ($K_D \sim 5$ nM), by further increasing the k_{on} . Because the higher k_{on} could result in mass transfer limiting binding, we confirmed that the kinetic measurement for this variant was not substantially affected by varying levels of immobilization (Figure 3-figure supplement 1). The affinity of the Beta (K417N/E484K/N501Y) and Gamma (K417T/E484K/N501Y) RBD variants for ACE2 increased by 3.7 and 5.3 fold, respectively, relative to wild type RBD, by both increasing the k_{on} and decreasing the k_{off} rate constants.

We next examined whether the effects of the mutations were additive, as is typically the case for multiple mutations at protein/protein interfaces (Wells, 1990). To do this we converted the changes in K_D to changes in binding energy ($\Delta\Delta G$, Table 2) and examined whether the $\Delta\Delta G$ measured for RBD variants with multiple mutations was equal to the sum of the $\Delta\Delta G$ values measured for the individual RBD mutants. This was indeed the case (Figure 3D), indicating that the effects on each mutation are independent. This is consistent with them being spaced well apart within the interface (Figure 1C), and validates the accuracy of the affinity measurements.

The effects of ACE2 mutations

We next examined the effects of mutations of ACE2 (S19P and K26R) on binding to both wild type and common variants of RBD (Figure 4, Figure 4-figure supplement 1, and Table 1).

Both S19P and K26R increased the affinity of WT RBD binding by ~ 3.7 and ~ 2.4 fold (Figure 4A). These increases in affinity were the result of both increases in the k_{on} and decreases in the k_{off} .

Finally, we looked for interactions between RBD and ACE2 mutations by measuring the effects of the ACE2 mutations on binding to all mutant forms of RBD (Table 1). After converting changes in K_D to $\Delta\Delta G$ (Table 2) we examined whether $\Delta\Delta G$ measured for a given ACE2 variant/RBD variant interaction was equal to the sum of the $\Delta\Delta G$ measured for ACE2 variant/RBD WT and ACE WT/RBD variant interactions. This is depicted as the difference between the measured and predicted $\Delta\Delta G$ for interactions between ACE2 and RBD variants ($\Delta\Delta\Delta G$ in Figure 4B and C). In most cases $\Delta\Delta\Delta G$ values were close to zero, indicating that the effects of these mutations were largely independent. The one exception was the combination of ACE2 S19P and RBD S477N variants, where the measured value was significantly lower than the predicted value (Figure 4B), indicating that these mutations were not independent. This is consistent with the fact that the ACE2 residue S19 is adjacent to RBD residue S477 in the contact interface (Figure 1C). An important consequence of this is that the S477N mutation increased the affinity of RBD for ACE2 WT but decreased its affinity for ACE2 S19P.

Discussion

While our finding that the SARS-CoV-2 RBD binds ACE2 with an affinity of K_D 74 nM at 37°C is consistent with previous studies (K_D 6 to 133 nM) (Laffeber et al., 2021; Lei et al., 2020; Liu et al., 2021; Shang et al., 2020; Supasa et al., 2021; Wrapp et al., 2020; Zhang et al., 2021, 2020), the rate constants that we measured (k_{on} $0.9 \mu M^{-1}.s^{-1}$ and k_{off} $0.067 s^{-1}$) were faster than all previous reports. One likely reason for this is that previous measurements were performed at a lower temperature, which almost always decreases rate constants. While some studies stated that binding constants were measured at 25°C (Laffeber et al., 2021; Zhang et al., 2020), most studies did not report the temperature, suggesting that they were performed at room temperature or the standard instrument temperature (20-25°C). A

210 second likely reason is that previous kinetic studies were performed under conditions in
 211 which the rate of diffusion of soluble molecule to the sensor surface limits the association
 212 rate, and rebinding of dissociated molecules to the surface reduces the measured
 213 dissociation rate. These are known pitfalls of both techniques used in these studies, surface
 214 plasmon resonance (Myszka, 1997) and bilayer interferometry (Abdiche et al., 2008). In the
 215 present study we avoided these issues by immobilizing a very low level of ligand on the
 216 sensor surface. A third possible reason is that the proteins were aggregated, which can
 217 cause problems even when aggregates are a very minor contaminant (van der Merwe and
 218 Barclay, 1996). The presence of aggregates results in complex binding kinetics, which can be
 219 excluded if the simple 1:1 Langmuir binding model fits the kinetic data. While this was
 220 demonstrated in the present study, and some previous studies (Shang et al., 2020; Wrapp et
 221 al., 2020; Zhang et al., 2021), such fits were not shown in all studies, one of which reported
 222 more than 20 fold slower kinetics than reported here (Lei et al., 2020; Supasa et al., 2021).

223 The RBD mutations that we selected for analysis have all emerged independently and
 224 became dominant in a region at least once in different lineages, suggesting that they
 225 provide a selective advantage. Our finding that the N501Y, E484K, and S477N all increase
 226 the binding affinity of RBD for ACE2 raises the question as to whether this contributed to
 227 their selection. Several lines of evidence suggest that enhancing the Spike/ACE2 interaction
 228 would be advantageous for the virus. Firstly, the virus has spread only very recently to
 229 humans from another mammalian host, providing insufficient time for optimization of the
 230 affinity. Secondly, epidemiological studies have suggested that the Alpha variant, which has
 231 the N501Y mutation, has enhanced transmissibility (Volz et al., 2021b; Washington et al.,
 232 2021). Finally, a SARS-CoV-2 variant with the Spike mutation D614G, which increases its
 233 activity by stabilizing it following furin cleavage (Zhang et al., 2021, 2020), rapidly became
 234 dominant globally after it emerged (Korber et al., 2020; Volz et al., 2021a). Taken together,
 235 these findings suggest that the WT Spike/ACE2 interaction is limiting for transmission, and
 236 that mutations which enhance it, including the N501Y, E484K, and S477N mutations, could
 237 provide a selective advantage by increasing transmissibility. This raises two questions.
 238 Firstly, will other RBD mutations appear in SARS-CoV-2 which further enhance transmission?
 239 This seems likely, given that a large number of RBD mutations have been identified that
 240 increase the RBD/ACE2 affinity (Starr et al., 2020; Zahradník et al., 2021). Secondly, will

combinations of existing mutations be selected because they further increase the affinity? While the appearance E484K together with N501Y in three lineages (Alpha, Beta, and Gamma) supports this, it is also possible that E484K was selected because it disrupts antibody neutralization, as discussed below.

Our affinity and kinetic data on RBD variants are broadly consistent with some (Laffebert et al., 2021; Liu et al., 2021), but not all (Dejnirattisai et al., 2021; D. Zhou et al., 2021), recent reports on the K417T/N, N501Y, and E484K variants. One caveat to our study is that we used monomeric forms of RBD and ACE2. The native Spike protein is a trimer and has several other domains, including the nearby N-terminal domain, and the native ACE2 protein can exist as a dimer (Yan et al., 2020). Because of these differences, our analysis may not detect the full effects of RBD and ACE2 mutations on the Spike/ACE2 interaction. A second caveat is that we have not examined the effect of these mutations on viral attachment to cells.

Studies of other enveloped viruses, including SARS-CoV, suggest that increases in affinity of viral ligands for their cellular receptors can increase cell infection and disease severity (Hasegawa et al., 2007; Li et al., 2005). One study found that increasing this affinity enabled the virus to infect cells with lower receptor surface density (Hasegawa et al., 2007). It follows that increases in affinity could increase the number of host tissues infected, which could increase the severity of disease (Cao and Li, 2020) and/or increase the viral load in the upper respiratory tract (Hoffmann et al., 2020; Wölfel et al., 2020), thereby increasing spread.

Another mechanism by which mutations of RBD could provide a selective advantage is through evasion of immune responses. This is supported by the observation that neutralizing antibodies present in those infected by or vaccinated against SARS-CoV-2 primarily target the RBD (Garcia-Beltran et al., 2021; Greaney et al., 2021a; Rogers et al., 2020). Furthermore, two variants with RBD mutations that abrogate antibody neutralization, Beta and Gamma, became dominant in regions with very high levels of prior SARS-CoV-2 infection (Cele et al., 2021; Dejnirattisai et al., 2021; Hoffmann et al., 2021; Sabino et al., 2021; Tegally et al., 2021; D. Zhou et al., 2021). Both lineages include the N501Y mutation, but this appears to have modest effects on antibody neutralization (Greaney et al., 2021a, 2021b). In contrast, the E484K mutation, also present in both variants, potentially disrupts antibody neutralization (Greaney et al., 2021a, 2021b). Our

finding that the K417N/T mutations present in Beta and Gamma variants decrease the affinity of RBD for ACE2 suggests that they were selected because they facilitate immune escape. Indeed, mutations of K417 can block antibody neutralization, albeit less effectively than E484K (Greaney et al., 2021a, 2021b; Wang et al., 2021). It is notable that these affinity-reducing K417N/T mutations have only emerged together with mutations (N501Y and E484K) that increase the affinity of RBD for ACE2, suggesting a cooperative effect between mutations that enhance immune escape and mutations that increase affinity.

The effect of the increased affinity for SARS-CoV-2 Spike RBD of the K26R and S19P ACE2 mutants is less clear. The evidence summarised above that WT RBD/ACE2 binding is limiting for SARS-CoV-2 transmission, suggest that carriers of these ACE2 variants will be at greater risk of infection and/or severe disease. However, in contrast to SARS-CoV-2 RBD mutations, the effects of ACE2 variants are primarily relevant to the carriers of these mutations. A preliminary analysis (MacGowan et al., 2021) suggests that the carriers of the K26R ACE allele might be at increased risk of severe disease, but the findings did not reach statistical significance, and further studies are required.

The interaction that we identified between the RBD S477N and ACE2 S19P mutants highlights the importance of considering variation in the host population when studying the evolution of viral variants. In this case, the opposite effect of the RBD S477N mutation on its affinity for ACE2 S19P (decreased) compared with ACE2 WT (increased), suggests that this RBD variant may have a selective disadvantage amongst carriers of the ACE2 S19P variant, in contrast to those with ACE2 WT, where it appears to be advantageous. However, the low frequency of this variant means that this is unlikely to be important at a population level and will be difficult to detect.

It is noteworthy that the two most common ACE2 variants are in positions on ACE2 with no known functional activity. This raises the question as to whether these mutations are a remnant of historic adaption to pathogens that utilised this portion of ACE2. The fact that ACE2 S19P mutation is largely confined to African/African-American populations, suggests that it is more recent than K26R and/or selected by pathogen(s) confined to the African continent.

Key Resources Table				
Reagent type (species) or resource	Designation	Source or reference	Identifiers	Additional information
transfected construct (human)	ACE2 WT	Oxford Protein Production Facility-UK	pOPINTTGneo_ACE2-BAP	
transfected construct (human)	ACE2 S19P; ACE2 K26R	This paper		Available from authors
transfected construct (<i>SARS-CoV-2</i>)	RBD WT	BEI Resources, NIH	NR-52309	pCAGG plasmid
transfected construct (<i>SARS-CoV-2</i>)	RBD K417N; RBD RBD K417T; RBD S477N; RBD E484K; RBD N501Y; RBD K417N/E484K; RBD K417T/E484K; RBD beta; RBD gamma	This paper		pCAGG plasmid. Available from authors
transfected construct (human)	pTT3-BirA-FLAG	Addgene	RRID:Addgene_64395	Cotransfected for in-cell biotinylation
peptide, recombinant protein	ACE2 WT; ACE2 S19P; ACE2 K26R	This paper		Expressed in HEK293 cells and purified
peptide, recombinant protein	RBD WT; RBD K417N; RBD K417T; RBD S477N; RBD E484K; RBD N501Y; RBD K417N/E484K; RBD K417T/E484K; RBD beta; RBD gamma	This paper		Expressed in HEK293 cells and purified

antibody	anti-human ACE2 (mouse monoclonal)	NOVUS Biologicals	AC384	(5 µg/mL)
cell line (human)	FreeStyle™ HEK293F Cells	ThermoFisher Scientific	RRID:CVCL_D603	
chemical compound, drug	FreeStyle™ MAX Reagent	ThermoFisher	16447100	
chemical compound, drug	FreeStyle™ 293 Expression Medium	ThermoFisher	12338018	
commercial assay or kit	QuikChange II XL	Agilent	200521	
commercial assay or kit	Amine coupling kit	Cytiva	BR100050	
software, algorithm	GraphPad	Prism	Version 9	
Other	CM5 sensor chips	Cytiva	29149603	

ACE2 and RBD variant constructs

The plasmid used to express soluble ACE2 WT (pOPINTTNeo_ACE2-BAP), which was kindly provided by Ray Owens (Oxford Protein Production Facility-UK), encoded the following protein:

STIEEQAKTFLDKFNHEAEDLFYQSSLASWNYNTNITEENVQNMNNAGDKWSAFLKEQSTLAQMYPLQ
EIQNLTVKLQLQALQQNGSSVLSEDKSKRLNTILNTMSTIYSTGKVCNPDNPQECLLLEPGLNEIMANSLD
YNERLWAWESWRSEVGKQLRPLYEEYVVLKNEMARANHYEDYGDYWRGDYEVNGVDGYDYSRGQLI
EDVEHTFEEIKPLYEHLHAYVRAKLMNAYPSYISPIGCLPAHLLGDMWGRFWTNLYSLTVPFGQKPNIDV
TDAMVDQAWDAQRIFKEAEKFFVSVGLPNMTQGFWENSMLTDPGNVQKAVCHPTAWDLGKGFRI

313 LMCTKVTMDDFLTAHHEMGHIQYDMAYAAQPFLLRNGANEGFHEAVGEIMSLSAATPKHLKSIGLLSP
314 DFQEDNETEINFLKQALTIVGTLPFTYMLEKWRWMVFKGEIPKDQWMKKWWEMKREIVGVVEPVP
315 HDETYCDPASLFHVSNDYSFIRYYTRTLYQFQFQEALCQAAKHEGPLHKCDISNSTEAGQKLFNMLRLGK
316 SEPWTLALENVVGAKNMNVRPLLNYFEPLFTWLKDQNKNSFVGWSTDWSPYADLNDIFEAQKIEWHE
317 KHHHHHH

318 The carboxy-terminal end has a biotin acceptor peptide (underlined) followed by an
319 oligohistidine tag.

320 The pCAGG plasmid used to express the RBD WT construct (Amanat et al., 2020) encoded
321 the following protein:

322 RVQPTESIVRFPNITNLCPFGEVFNATRFASVYAWNRKRISNCVADYSVLYNSASFSTFKCYGVSPTKLND
323 LCFTNVYADSFVIRGDEVQRQIAPGQTGKIADYNYKLPDDFTGCVIAWNSNNLDSKVGGNYNLYRLFRKS
324 NLKPFERDISTEIYQAGSTPCNGVEGFNCYFPLQSYGFQPTNGVGYQPYRVVVLSELLHAPATVCGPKKS
325 TNLVKNKCVNFHHHHHH

326 The carboxy-terminal end has an oligohistidine tag.

327 ACE2 and RBD point mutations were introduced into these plasmid constructs using the
328 Agilent QuikChange II XL Site-Directed Mutagenesis Kit following the manufacturer's
329 instructions. The primers were designed using the Agilent QuikChange primer design web
330 program.

331 **HEK293F cell transfection**

332 Cells were grown in FreeStyle™ 293 Expression Medium (ThermoFisher Scientific, 12338018)
333 in a 37 °C incubator with 8% CO₂ on a shaking platform at 130 rpm. Cells were passaged
334 every 2-3 days with the suspension volume always kept below 33.3% of the total flask
335 capacity. The cell density was kept between 0.5 and 2 million per ml. Before transfection
336 cells were counted to check that cell viability was above 95% and the density was adjusted
337 to 1.0 million per ml. For 100 ml transfection, 100 µl FreeStyle™ MAX Reagent
338 (ThermoFisher Scientific, 16447100) was mixed with 2 ml Opti-MEM (ThermoFisher
339 Scientific, 51985034) for 5 minutes. During this incubation 100 µg of expression plasmid was
340 mixed with 2 ml Opti-MEM (or in situ biotinylation of ACE2 90 µg of expression plasmid was
341 mixed with 10 µg of expression plasmid encoding the BirA enzyme). The DNA was then
342 mixed with the MAX Reagent and incubated for 25 minutes before being added to the cell

culture. For ACE2 in situ biotinylation, biotin was added to the cell culture at a final concentration of 50 μ M. The culture was left for 5 days for protein expression to take place.

Protein purification

Cells were harvested by centrifugation and the supernatant collected and filtered through a 0.22 μ m filter. Imidazole was added to a final concentration of 10 mM and PMSF added to a final concentration of 1 mM; 1 ml of Ni-NTA Agarose (Qiagen; 30310) was added per 100 ml of supernatant and the mix was left on a rolling platform at 4 °C overnight. The mix was poured through a gravity flow column to collect the Ni-NTA Agarose. The Ni-NTA Agarose was washed 3 times with 25 ml of wash buffer (50 mM NaH_2PO_4 , 300 mM NaCl and 20 mM imidazole at pH 8). The protein was eluted with elution buffer (50 mM NaH_2PO_4 , 300 mM NaCl and 250 mM imidazole at pH 8). The protein was concentrated, and buffer exchanged into size exclusion buffer (25 mM NaH_2PO_4 , 150 mM NaCl at pH 7.5) using a protein concentrator with a 10,000 molecular weight cut-off. The protein was concentrated down to less than 500 μ l and loading onto a Superdex 200 10/300 GL (Cytiva, 17-5175-01) size exclusion column (Figure 2-figure supplement 1). Fractions corresponding to the desired peak were pooled and frozen at -80 °C. Samples from all observed peaks were analysed on a reducing SDS-PAGE gel (Figure 2-figure supplement 1).

Surface plasmon resonance

RBD binding to ACE2 was analysed on a Biacore T200 instrument (Cytiva™) at 37°C and a flow rate of 30 μ l/min. Running buffer was HBS-EP (Cytiva™, BR100669). Streptavidin was coupled to a CM5 sensor chip (Cytiva™, 29149603) using an amine coupling kit (Cytiva™, BR100050) to near saturation, typically 10000-12000 response units (RU). Biotinylated ACE2 WT and variants were injected into the experimental flow cells (FC2–FC4) for different lengths of time to produce desired immobilisation levels (20–800 RU). FC1 was used as a reference and contained streptavidin only. Excess streptavidin was blocked with two 40 s injections of 250 μ M biotin (Avidity™). Before RBD injections, the chip surface was conditioned with 8 injections of the running buffer. A dilution series of RBD was then injected in all FCs. Buffer alone was injected after every 2 or 3 RBD injections. The length of all injections was 30 s, and dissociation was monitored for 180-670 s. The background response measured in FC1 was subtracted from the response in the other three FCs. In

addition, the responses measured during buffer injections closest in time were subtracted. Such double-referencing improves data quality when binding responses are low as needed to obtain accurate kinetic data (Myszka, 1999). At the end of each experiment an ACE2-specific mouse monoclonal antibody (NOVUS Biologicals, AC384) was injected at 5 µg/ml for 10 minutes to confirm the presence and relative amounts of immobilized ACE2.

Data analysis

Double-referenced binding data was fitted using GraphPad Prism. The k_{off} was determined by fitting a mono-exponential decay curve to data from the dissociation phase of each injection. The k_{off} from four to six RBD injections was averaged (Figure 2-figure supplement 2A). The k_{on} was determined by first fitting a mono-exponential association curve to data from the association phase, yielding the k_{obs} , and then plotting the k_{obs} vs the concentration of RBD and performing a linear fit of the equation $k_{obs} = k_{on} * [RBD] + k_{off}$ to this data (Figure 2-figure supplement 2B), using the k_{off} determined as above to constrain the fit.

The K_D was either calculated (calculated $K_D = k_{off}/k_{on}$) or measured directly (equilibrium K_D) as follows. Equilibrium binding levels at a given [RBD] were determined from the fit of the mono-exponential association phase model to the association phase data. These equilibrium binding levels were plotted against [RBD] and a fit of the simple 1:1 Langmuir binding model to this data was used to determine the equilibrium K_D (Figure 2D).

ΔG for each affinity measurement was calculated from the relationship $\Delta G = R * T * \ln K_D$, where $R = 1.987 \text{ cal mol}^{-1} \text{ K}^{-1}$, $T = 310.18 \text{ K}$, and K_D is in units M. $\Delta \Delta G$ values (Table 2 and Figure 3D) were calculated for each mutant from the relationship $\Delta \Delta G = \Delta G_{WT} - \Delta G_M$. The predicted $\Delta \Delta G$ for interactions with multiple mutants were calculated by adding the single mutant $\Delta \Delta G$ values (Figure 3D). The difference between the measured and predicted $\Delta \Delta G$ ($\Delta \Delta \Delta G$) for interactions between the ACE2 and RBD mutants was calculated as $\Delta \Delta \Delta G = \text{measured } \Delta \Delta G - \text{predicted } \Delta \Delta G$ (Figure 4B).

All errors represent standard deviations and errors for calculated values were determined by error propagation.

Acknowledgments

401 We thank Johannes Pettmann for help with protein expression and Anna Huhn for help with
402 data analysis. OD is supported by a Wellcome Trust Senior Fellowship in Basic Biomedical
403 Sciences (207537/Z/17/Z828). SM and GB are supported by Biotechnology and Biological
404 Sciences Research Council Grants (BB/J019364/1 and BB/R014752/1) and a Wellcome Trust
405 Biomedical Resources Grant (101651/Z/13/Z).

406 **Conflicts of interest**

407 PAV owns BioNTech SE stock. The authors declare no other conflicts of interest.

References

- Abdiche Y, Malashock D, Pinkerton A, Pons J. 2008. Determining kinetics and affinities of protein interactions using a parallel real-time label-free biosensor, the Octet. *Anal Biochem* **377**:209–217. doi:10.1016/j.ab.2008.03.035
- Agius R, Torchala M, Moal IH, Fernández-Recio J, Bates PA. 2013. Characterizing Changes in the Rate of Protein-Protein Dissociation upon Interface Mutation Using Hotspot Energy and Organization. *Plos Comput Biol* **9**:e1003216. doi:10.1371/journal.pcbi.1003216
- Amanat F, Stadlbauer D, Strohmeier S, Nguyen THO, Chromikova V, McMahon M, Jiang K, Arunkumar GA, Jurczyszak D, Polanco J, Bermudez-Gonzalez M, Kleiner G, Aydililo T, Miorin L, Fierer DS, Lugo LA, Kojic EM, Stoeve J, Liu STH, Cunningham-Rundles C, Felgner PL, Moran T, García-Sastre A, Caplivski D, Cheng AC, Kedzierska K, Vapalahti O, Hepojoki JM, Simon V, Krammer F. 2020. A serological assay to detect SARS-CoV-2 seroconversion in humans. *Nat Med* **26**:1033–1036. doi:10.1038/s41591-020-0913-5
- Cao W, Li T. 2020. COVID-19: towards understanding of pathogenesis. *Cell Res* **30**:367–369. doi:10.1038/s41422-020-0327-4
- Cele S, Gazy I, Team C-K, NGS-SA, Jackson L, Hwa S-H, Tegally H, Lustig G, Giandhari J, Pillay S, Wilkinson E, Naidoo Y, Karim F, Ganga Y, Khan K, Bernstein M, Balazs AB, Gosnell BI, Hanekom W, Moosa M-YS, Lessells RJ, Oliveira T de, Sigal A. 2021. Escape of SARS-CoV-2 501Y.V2 from neutralization by convalescent plasma. *Nature* 1–9. doi:10.1038/s41586-021-03471-w
- Darby AC, Hiscox JA. 2021. Covid-19: variants and vaccination. *Bmj* **372**:n771. doi:10.1136/bmj.n771
- Davies NG, Edmunds WJ. 2021. Estimated transmissibility and impact of SARS-CoV-2 lineage B.1.1.7 in England. *Science*. doi:10.1126/science. abg3055
- Dejnirattisai W, Zhou D, Supasa P, Liu C, Mentzer AJ, Ginn HM, Zhao Y, Duyvesteyn HME, Tuekprakhon A, Nutalai R, Wang B, Paesen GC, López-Camacho C, Slon-Campos J, Walter TS, Skelly D, Clemens SAC, Naveca FG, Nascimento V, Nascimento F, Costa CF da, Resende PC, Pauvolid-Correa A, Siqueira MM, Dold C, Levin R, Dong T, Pollard AJ, Knight JC, Crook D, Lambe T, Clutterbuck E, Bibi S, Flaxman A, Bittaye M, Belij-Rammerstorfer S, Gilbert S, Carroll MW, Klenerman P, Barnes E, Dunachie SJ, Paterson NG, Williams MA, Hall DR, Hulswit RJG, Bowden TA, Fry EE, Mongkolsapaya J, Ren J, Stuart DI, Screaton GR. 2021. Antibody evasion by the P.1 strain of SARS-CoV-2. *Cell*. doi:10.1016/j.cell.2021.03.055
- Garcia-Beltran WF, Lam EC, Denis KSt, Nitido AD, Garcia ZH, Hauser BM, Feldman J, Pavlovic MN, Gregory DJ, Poznansky MC, Sigal A, Schmidt AG, Iafrate AJ, Naranbhai

447 V, Balazs AB. 2021. Multiple SARS-CoV-2 variants escape neutralization by vaccine-
448 induced humoral immunity. *Cell*. doi:10.1016/j.cell.2021.03.013

449 Greaney AJ, Loes AN, Crawford KHD, Starr TN, Malone KD, Chu HY, Bloom JD. 2021a.
450 Comprehensive mapping of mutations in the SARS-CoV-2 receptor-binding domain that
451 affect recognition by polyclonal human plasma antibodies. *Cell Host Microbe* **29**:463-
452 476.e6. doi:10.1016/j.chom.2021.02.003

453 Greaney AJ, Starr TN, Gilchuk P, Zost SJ, Binshtein E, Loes AN, Hilton SK, Huddleston J,
454 Eguia R, Crawford KHD, Dingens AS, Nargi RS, Sutton RE, Suryadevara N, Rothlauf
455 PW, Liu Z, Whelan SPJ, Carnahan RH, Crowe JE, Bloom JD. 2021b. Complete Mapping
456 of Mutations to the SARS-CoV-2 Spike Receptor-Binding Domain that Escape Antibody
457 Recognition. *Cell Host Microbe* **29**:44-57.e9. doi:10.1016/j.chom.2020.11.007

458 Hadfield J, Megill C, Bell SM, Huddleston J, Potter B, Callender C, Sagulenko P, Bedford T,
459 Neher RA. 2018. Nextstrain: real-time tracking of pathogen evolution. *Bioinformatics*
460 **34**:4121–4123. doi:10.1093/bioinformatics/bty407

461 Hasegawa K, Hu C, Nakamura T, Marks JD, Russell SJ, Peng K-W. 2007. Affinity
462 Thresholds for Membrane Fusion Triggering by Viral Glycoproteins ▽. *J Virol* **81**:13149–
463 13157. doi:10.1128/jvi.01415-07

464 Hodcroft EB. 2021. CoVariants: SARS-CoV-2 Mutations and Variants of Interest.
465 <https://covariants.org/>

466 Hoffmann M, Arora P, Groß R, Seidel A, Hörnich BF, Hahn AS, Krüger N, Graichen L,
467 Hofmann-Winkler H, Kempf A, Winkler MS, Schulz S, Jäck H-M, Jahrsdörfer B,
468 Schrezenmeier H, Müller M, Kleger A, Münch J, Pöhlmann S. 2021. SARS-CoV-2
469 variants B.1.351 and P.1 escape from neutralizing antibodies. *Cell*.
470 doi:10.1016/j.cell.2021.03.036

471 Hoffmann M, Kleine-Weber H, Schroeder S, Krüger N, Herrler T, Erichsen S, Schiergens
472 TS, Herrler G, Wu N-H, Nitsche A, Müller MA, Drosten C, Pöhlmann S. 2020. SARS-
473 CoV-2 Cell Entry Depends on ACE2 and TMPRSS2 and Is Blocked by a Clinically
474 Proven Protease Inhibitor. *Cell*. doi:10.1016/j.cell.2020.02.052

475 Karczewski KJ, Francioli LC, Tiao G, Cummings BB, Alföldi J, Wang Q, Collins RL,
476 Laricchia KM, Ganna A, Birnbaum DP, Gauthier LD, Brand H, Solomonson M, Watts
477 NA, Rhodes D, Singer-Berk M, England EM, Seaby EG, Kosmicki JA, Walters RK,
478 Tashman K, Farjoun Y, Banks E, Poterba T, Wang A, Seed C, Whiffin N, Chong JX,
479 Samocha KE, Pierce-Hoffman E, Zappala Z, O'Donnell-Luria AH, Minikel EV, Weisburd
480 B, Lek M, Ware JS, Vittal C, Armean IM, Bergelson L, Cibulskis K, Connolly KM,
481 Covarrubias M, Donnelly S, Ferriera S, Gabriel S, Gentry J, Gupta N, Jeandet T, Kaplan
482 D, Llanwarne C, Munshi R, Novod S, Petrillo N, Roazen D, Ruano-Rubio V, Saltzman A,
483 Schleicher M, Soto J, Tibbetts K, Tolonen C, Wade G, Talkowski ME, Salinas CAA,
484 Ahmad T, Albert CM, Ardissino D, Atzmon G, Barnard J, Beaugerie L, Benjamin EJ,
485 Boehnke M, Bonnycastle LL, Bottinger EP, Bowden DW, Bown MJ, Chambers JC, Chan
486 JC, Chasman D, Cho J, Chung MK, Cohen B, Correa A, Dabelea D, Daly MJ, Darbar D,
487 Duggirala R, Dupuis J, Ellinor PT, Elosua R, Erdmann J, Esko T, Färkkilä M, Florez J,
488 Franke A, Getz G, Glaser B, Glatt SJ, Goldstein D, Gonzalez C, Groop L, Haiman C,

489 Hanis C, Harms M, Hiltunen M, Holi MM, Hultman CM, Kallela M, Kaprio J, Kathiresan
 490 S, Kim B-J, Kim YJ, Kirov G, Kooner J, Koskinen S, Krumholz HM, Kugathasan S,
 491 Kwak SH, Laakso M, Lehtimäki T, Loos RJF, Lubitz SA, Ma RCW, MacArthur DG,
 492 Marrugat J, Mattila KM, McCarroll S, McCarthy MI, McGovern D, McPherson R, Meigs
 493 JB, Melander O, Metspalu A, Neale BM, Nilsson PM, O'Donovan MC, Ongur D, Orozco
 494 L, Owen MJ, Palmer CNA, Palotie A, Park KS, Pato C, Pulver AE, Rahman N, Remes
 495 AM, Rioux JD, Ripatti S, Roden DM, Saleheen D, Salomaa V, Samani NJ, Scharf J,
 496 Schunkert H, Shoemaker MB, Sklar P, Soininen H, Sokol H, Spector T, Sullivan PF,
 497 Suvisaari J, Tai ES, Teo YY, Tiinamaija T, Tsuang M, Turner D, Tusie-Luna T,
 498 Vartiainen E, Vawter MP, Ware JS, Watkins H, Weersma RK, Wessman M, Wilson JG,
 499 Xavier RJ, Neale BM, Daly MJ, MacArthur DG. 2020. The mutational constraint
 500 spectrum quantified from variation in 141,456 humans. *Nature* **581**:434–443.
 501 doi:10.1038/s41586-020-2308-7

502 Korber B, Fischer WM, Gnanakaran S, Yoon H, Theiler J, Abfalterer W, Hengartner N,
 503 Giorgi EE, Bhattacharya T, Foley B, Hastie KM, Parker MD, Partridge DG, Evans CM,
 504 Freeman TM, Silva TI de, Group SC-19 G, Group M of SC-19 G, Angyal A, Brown RL,
 505 Carrilero L, Green LR, Groves DC, Johnson KJ, Keeley AJ, Lindsey BB, Parsons PJ,
 506 Raza M, Rowland-Jones S, Smith N, Tucker RM, Wang D, Wyles MD, McDanal C, Perez
 507 LG, Tang H, Moon-Walker A, Whelan SP, LaBranche CC, Saphire EO, Montefiori DC.
 508 2020. Tracking Changes in SARS-CoV-2 Spike: Evidence that D614G Increases
 509 Infectivity of the COVID-19 Virus. *Cell* **182**:812-827.e19. doi:10.1016/j.cell.2020.06.043

510 Laffebber C, Koning K de, Kanaar R, Lebbink JHG. 2021. Experimental Evidence for
 511 Enhanced Receptor Binding by Rapidly Spreading SARS-CoV-2 Variants. *J Mol Biol*
 512 **433**:167058. doi:10.1016/j.jmb.2021.167058

513 Lan J, Ge J, Yu J, Shan S, Zhou H, Fan S, Zhang Q, Shi X, Wang Q, Zhang L, Wang X.
 514 2020. Structure of the SARS-CoV-2 spike receptor-binding domain bound to the ACE2
 515 receptor. *Nature* **581**:215–220. doi:10.1038/s41586-020-2180-5

516 Lei C, Qian K, Li T, Zhang S, Fu W, Ding M, Hu S. 2020. Neutralization of SARS-CoV-2
 517 spike pseudotyped virus by recombinant ACE2-Ig. *Nat Commun* **11**:2070.
 518 doi:10.1038/s41467-020-16048-4

519 Li W, Zhang C, Sui J, Kuhn JH, Moore MJ, Luo S, Wong S, Huang I, Xu K, Vasilieva N,
 520 Murakami A, He Y, Marasco WA, Guan Y, Choe H, Farzan M. 2005. Receptor and viral
 521 determinants of SARS-coronavirus adaptation to human ACE2. *Embo J* **24**:1634–1643.
 522 doi:10.1038/sj.emboj.7600640

523 Liu H, Zhang Q, Wei P, Chen Z, Aviszus K, Yang J, Downing W, Jiang C, Liang B, Reynoso
 524 L, Downey GP, Frankel SK, Kappler J, Marrack P, Zhang G. 2021. The basis of a more
 525 contagious 501Y.V1 variant of SARS-CoV-2. *Cell Res* **31**:720–722. doi:10.1038/s41422-
 526 021-00496-8

527 MacGowan SA, Barton MI, Kutuzov M, Dushek O, Merwe PA van der, Barton GJ. 2021.
 528 Missense variants in human ACE2 modify binding to SARS-CoV-2 Spike. *bioRxiv*.
 529 doi:10.1101/2021.05.21.445118

530 Madhi SA, Baillie V, Cutland CL, Voysey M, Koen AL, Fairlie L, Padayachee SD, Dheda K,
531 Barnabas SL, Bhorat QE, Briner C, Kwatra G, Ahmed K, Aley P, Bhikha S, Bhiman JN,
532 Bhorat AE, Plessis J du, Esmail A, Groenewald M, Horne E, Hwa S-H, Jose A, Lambe T,
533 Laubscher M, Malahleha M, Masenya M, Masilela M, McKenzie S, Molapo K, Moultrie
534 A, Oelofse S, Patel F, Pillay S, Rhead S, Rodel H, Rossouw L, Taoushanis C, Tegally H,
535 Thombrayil A, Eck S van, Wibmer CK, Durham NM, Kelly EJ, Villafana TL, Gilbert S,
536 Pollard AJ, Oliveira T de, Moore PL, Sigal A, Izu A, Group N-SGWC. 2021a. Efficacy of
537 the ChAdOx1 nCoV-19 Covid-19 Vaccine against the B.1.351 Variant. *New Engl J Med*.
538 doi:10.1056/nejmoa2102214

539 Madhi SA, Baillie V, Cutland CL, Voysey M, Koen AL, Fairlie L, Padayachee SD, Dheda K,
540 Barnabas SL, Bhorat QE, Briner C, Kwatra G, NGS-SA, team W-VC, Ahmed K, Aley P,
541 Bhikha S, Bhiman JN, Bhorat AE, Plessis J du, Esmail A, Groenewald M, Horne E, Hwa
542 S-H, Jose A, Lambe T, Laubscher M, Malahleha M, Masenya M, Masilela M, McKenzie
543 S, Molapo K, Moultrie A, Oelofse S, Patel F, Pillay S, Rhead S, Rodel H, Rossouw L,
544 Taoushanis C, Tegally H, Thombrayil A, Eck S van, Wibmer CK, Durham NM, Kelly EJ,
545 Villafana TL, Gilbert S, Pollard AJ, Oliveira T de, Moore PL, Sigal A, Izu A. 2021b.
546 Safety and efficacy of the ChAdOx1 nCoV-19 (AZD1222) Covid-19 vaccine against the
547 B.1.351 variant in South Africa. *medRxiv*. doi:10.1101/2021.02.10.21251247

548 Mahase E. 2021. Covid-19: Where are we on vaccines and variants? *Bmj* **372**:n597.
549 doi:10.1136/bmj.n597

550 Myszka DG. 1999. Improving biosensor analysis. *J Mol Recognit* **12**:279–284.
551 doi:10.1002/(sici)1099-1352(199909/10)12:5<279::aid-jmr473>3.0.co;2-3

552 Myszka DG. 1997. Kinetic analysis of macromolecular interactions using surface plasmon
553 resonance biosensors. *Curr Opin Biotech* **8**:50–57. doi:10.1016/s0958-1669(97)80157-7

554 Pettersen EF, Goddard TD, Huang CC, Couch GS, Greenblatt DM, Meng EC, Ferrin TE.
555 2004. UCSF Chimera—A visualization system for exploratory research and analysis. *J*
556 *Comput Chem* **25**:1605–1612. doi:10.1002/jcc.20084

557 Rambaut A, Holmes EC, O’Toole Á, Hill V, McCrone JT, Ruis C, Plessis L du, Pybus OG.
558 2020. A dynamic nomenclature proposal for SARS-CoV-2 lineages to assist genomic
559 epidemiology. *Nat Microbiol* **5**:1403–1407. doi:10.1038/s41564-020-0770-5

560 Richard D, Shaw LP, Lanfear R, Acman M, Owen CJ, Tan CC, Dorp L van, Balloux F. 2021.
561 A phylogeny-based metric for estimating changes in transmissibility from recurrent
562 mutations in SARS-CoV-2. *Biorxiv* 2021.05.06.442903. doi:10.1101/2021.05.06.442903

563 Rogers TF, Zhao F, Huang D, Beutler N, Burns A, He W, Limbo O, Smith C, Song G, Woehl
564 J, Yang L, Abbott RK, Callaghan S, Garcia E, Hurtado J, Parren M, Peng L, Ramirez S,
565 Ricketts J, Ricciardi MJ, Rawlings SA, Wu NC, Yuan M, Smith DM, Nemazee D, Teijaro
566 JR, Voss JE, Wilson IA, Andrabi R, Briney B, Landais E, Sok D, Jardine JG, Burton DR.
567 2020. Isolation of potent SARS-CoV-2 neutralizing antibodies and protection from
568 disease in a small animal model. *Science* **369**:956–963. doi:10.1126/science.abc7520

569 Sabino EC, Buss LF, Carvalho MPS, Prete CA, Crispim MAE, Fraiji NA, Pereira RHM,
570 Parag KV, Peixoto P da S, Kraemer MUG, Oikawa MK, Salomon T, Cucunuba ZM,

571 Castro MC, Santos AA de S, Nascimento VH, Pereira HS, Ferguson NM, Pybus OG,
572 Kucharski A, Busch MP, Dye C, Faria NR. 2021. Resurgence of COVID-19 in Manaus,
573 Brazil, despite high seroprevalence. *Lancet* **397**:452–455. doi:10.1016/s0140-
574 6736(21)00183-5

575 Sagulenko P, Puller V, Neher RA. 2018. TreeTime: Maximum-likelihood phylodynamic
576 analysis. *Virus Evol* **4**:vex042-. doi:10.1093/ve/vex042

577 SARS-CoV-2 Variants of concern and variants under investigation - GOV.UK. 2021.
578 [https://www.gov.uk/government/publications/covid-19-variants-genomically-confirmed-](https://www.gov.uk/government/publications/covid-19-variants-genomically-confirmed-case-numbers/variants-distribution-of-cases-data)
579 [case-numbers/variants-distribution-of-cases-data](https://www.gov.uk/government/publications/covid-19-variants-genomically-confirmed-case-numbers/variants-distribution-of-cases-data)

580 Schreiber G, Fersht AR. 1996. Rapid, electrostatically assisted association of proteins. *Nat*
581 *Struct Biol* **3**:427–431. doi:10.1038/nsb0596-427

582 Shang J, Ye G, Shi K, Wan Y, Luo C, Aihara H, Geng Q, Auerbach A, Li F. 2020. Structural
583 basis of receptor recognition by SARS-CoV-2. *Nature* **581**:221–224. doi:10.1038/s41586-
584 020-2179-y

585 Shu Y, McCauley J. 2017. GISAID: Global initiative on sharing all influenza data – from
586 vision to reality. *Eurosurveillance* **22**:30494. doi:10.2807/1560-7917.es.2017.22.13.30494

587 Starr TN, Greaney AJ, Hilton SK, Ellis D, Crawford KHD, Dingens AS, Navarro MJ, Bowen
588 JE, Tortorici MA, Walls AC, King NP, Velesler D, Bloom JD. 2020. Deep Mutational
589 Scanning of SARS-CoV-2 Receptor Binding Domain Reveals Constraints on Folding and
590 ACE2 Binding. *Cell* **182**:1295–1310.e20. doi:10.1016/j.cell.2020.08.012

591 Supasa P, Zhou D, Dejnirattisai W, Liu C, Mentzer AJ, Ginn HM, Zhao Y, Duyvesteyn
592 HME, Nutalai R, Tuekprakhon A, Wang B, Paesen GC, Slon-Campos J, López-Camacho
593 C, Hallis B, Coombes N, Bewley K, Charlton S, Walter TS, Barnes E, Dunachie SJ,
594 Skelly D, Lumley SF, Baker N, Shaik I, Humphries H, Godwin K, Gent N, Sienkiewicz
595 A, Dold C, Levin R, Dong T, Pollard AJ, Knight JC, Klennerman P, Crook D, Lambe T,
596 Clutterbuck E, Bibi S, Flaxman A, Bittaye M, Belij-Rammerstorfer S, Gilbert S, Hall DR,
597 Williams MA, Paterson NG, James W, Carroll MW, Fry EE, Mongkolsapaya J, Ren J,
598 Stuart DI, Screaton GR. 2021. Reduced neutralization of SARS-CoV-2 B.1.1.7 variant by
599 convalescent and vaccine sera. *Cell*. doi:10.1016/j.cell.2021.02.033

600 Tegally H, Wilkinson E, Giovanetti M, Iranzadeh A, Fonseca V, Giandhari J, Doolabh D,
601 Pillay S, San EJ, Msomi N, Mlisana K, Gottberg A von, Walaza S, Allam M, Ismail A,
602 Mohale T, Glass AJ, Engelbrecht S, Zyl GV, Preiser W, Petruccione F, Sigal A, Hardie D,
603 Marais G, Hsiao M, Korsman S, Davies M-A, Tyers L, Mudau I, York D, Maslo C,
604 Goedhals D, Abrahams S, Laguda-Akingba O, Alisoltani-Dehkordi A, Godzik A, Wibmer
605 CK, Sewell BT, Lourenço J, Alcantara LCJ, Pond SLK, Weaver S, Martin D, Lessells RJ,
606 Bhiman JN, Williamson C, Oliveira T de. 2021. Emergence of a SARS-CoV-2 variant of
607 concern with mutations in spike glycoprotein. *Nature* 1–8. doi:10.1038/s41586-021-
608 03402-9

609 van der Merwe PA van der, Barclay AN. 1996. Analysis of cell-adhesion molecule
610 interactions using surface plasmon resonance. *Current opinion in immunology* **8**:257–261.

611

612 V'kovski P, Kratzel A, Steiner S, Stalder H, Thiel V. 2021. Coronavirus biology and
 613 replication: implications for SARS-CoV-2. *Nat Rev Microbiol* **19**:155–170.
 614 doi:10.1038/s41579-020-00468-6

615 Volz E, Hill V, McCrone John T., Price A, Jorgensen D, O'Toole Á, Southgate J, Johnson
 616 Robert, Jackson B, Nascimento FF, Rey SM, Nicholls SM, Colquhoun RM, Filipe A da S,
 617 Shepherd J, Pascall DJ, Shah R, Jesudason N, Li K, Jarrett R, Pacchiarini N, Bull M,
 618 Geidelberg L, Siveroni I, Consortium C-U, Koshy C, Wise E, Cortes Nick, Lynch J, Kidd
 619 S, Mori M, Fairley DJ, Curran T, McKenna JP, Adams H, Fraser C, Golubchik T, Bonsall
 620 D, Moore Catrin, Caddy SL, Khokhar FA, Wantoch M, Reynolds N, Warne B,
 621 Maksimovic J, Spellman K, McCluggage K, John M, Beer R, Afifi S, Morgan S,
 622 Marchbank A, Price A, Kitchen C, Gulliver H, Merrick I, Southgate J, Guest M, Munn R,
 623 Workman T, Connor TR, Fuller W, Bresner C, Snell LB, Charalampous T, Nebbia G,
 624 Batra R, Edgeworth J, Robson SC, Beckett A, Loveson KF, Aanensen DM, Underwood
 625 AP, Yeats CA, Abudahab K, Taylor BEW, Menegazzo M, Clark G, Smith W, Khakh M,
 626 Fleming VM, Lister MM, Howson-Wells HC, Berry Louise, Boswell T, Joseph A,
 627 Willingham I, Bird P, Helmer T, Fallon K, Holmes C, Tang J, Raviprakash V, Campbell
 628 S, Sheriff N, Loose MW, Holmes N, Moore Christopher, Carlile M, Wright V, Sang F,
 629 Debebe J, Coll F, Signell AW, Betancor G, Wilson HD, Feltwell T, Houldcroft CJ,
 630 Eldirdiri S, Kenyon A, Davis T, Pybus O, Plessis L du, Zarebski A, Raghwan J, Kraemer
 631 M, Francois S, Attwood S, Vasylyeva T, Torok ME, Hamilton WL, Goodfellow IG, Hall
 632 G, Jahun AS, Chaudhry Y, Hosmillo M, Pinckert ML, Georgana I, Yakovleva A,
 633 Meredith LW, Moses S, Lowe H, Ryan F, Fisher CL, Awan AR, Boyes J, Breuer J, Harris
 634 KA, Brown JR, Shah D, Atkinson L, Lee JCD, Alcolea-Medina A, Moore N, Cortes
 635 Nicholas, Williams R, Chapman MR, Levett LJ, Heaney J, Smith DL, Bashton M, Young
 636 GR, Allan J, Loh J, Randell PA, Cox A, Madona P, Holmes A, Bolt F, Price J, Mookerjee
 637 S, Rowan A, Taylor GP, Ragonnet-Cronin M, Nascimento FF, Jorgensen D, Siveroni I,
 638 Johnson Rob, Boyd O, Geidelberg L, Volz EM, Brunner K, Smollett KL, Loman NJ,
 639 Quick J, McMurray C, Stockton J, Nicholls S, Rowe W, Poplawski R, Martinez-Nunez
 640 RT, Mason J, Robinson TI, O'Toole E, Watts J, Breen C, Cowell A, Ludden C, Sluga G,
 641 Machin NW, Ahmad SSY, George RP, Halstead F, Sivaprakasam V, Thomson EC,
 642 Shepherd JG, Asamaphan P, Niebel MO, Li KK, Shah RN, Jesudason NG, Parr YA, Tong
 643 L, Broos A, Mair D, Nichols J, Carmichael SN, Nomikou K, Aranday-Cortes E, Johnson
 644 N, Starinskij I, Filipe A da S, Robertson DL, Orton RJ, Hughes J, Vattipally S, Singer JB,
 645 Hale AD, Macfarlane-Smith LR, Harper KL, Taha Y, Payne BAI, Burton-Fanning S,
 646 Waugh S, Collins J, Eltringham G, Templeton KE, McHugh MP, Dewar R, Wastenge E,
 647 Dervisevic S, Stanley R, Prakash R, Stuart C, Elumogo N, Sethi DK, Meader EJ,
 648 Coupland LJ, Potter W, Graham C, Barton E, Padgett D, Scott G, Swindells E, Greenaway
 649 J, Nelson A, Yew WC, Silva PCR, Andersson M, Shaw R, Peto T, Justice A, Eyre D,
 650 Crooke D, Hoosdally S, Sloan TJ, Duckworth N, Walsh S, Chauhan AJ, Glaysher S,
 651 Bicknell K, Wyllie S, Butcher E, Elliott S, Lloyd A, Impey R, Levene N, Monaghan L,
 652 Bradley DT, Allara E, Pearson C, Muir P, Vipond IB, Hopes R, Pymont HM, Hutchings
 653 S, Curran MD, Parmar S, Lackenby A, Mbisa T, Platt S, Miah S, Bibby D, Manso C,
 654 Hubb J, Chand M, Dabrera G, Ramsay M, Bradshaw D, Thornton A, Myers R, Schaefer
 655 U, Groves N, Gallagher E, Lee D, Williams D, Ellaby N, Harrison I, Hartman H, Manesis
 656 N, Patel V, Bishop C, Chalker V, Osman H, Bosworth A, Robinson E, Holden MTG,
 657 Shaaban S, Birchley A, Adams A, Davies A, Gaskin A, Plimmer A, Gatica-Wilcox B,
 658 McKerr C, Moore Catherine, Williams C, Heyburn D, Lacy ED, Hilvers E, Downing F,

659 Shankar G, Jones H, Asad H, Coombes J, Watkins J, Evans JM, Fina L, Gifford L, Gilbert
 660 L, Graham L, Perry M, Morgan M, Bull M, Cronin M, Pacchiarini N, Craine N, Jones R,
 661 Howe R, Corden S, Rey S, Kumziene-Summerhayes S, Taylor S, Cottrell S, Jones S,
 662 Edwards S, O'Grady J, Page AJ, Wain J, Webber MA, Mather AE, Baker DJ, Rudder S,
 663 Yasir M, Thomson NM, Aydin A, Tedim AP, Kay GL, Trotter AJ, Gilroy RAJ, Alikhan
 664 N-F, Martins L de O, Le-Viet T, Meadows L, Kolyva A, Diaz M, Bell A, Gutierrez AV,
 665 Charles IG, Adriaenssens EM, Kingsley RA, Casey A, Simpson DA, Molnar Z,
 666 Thompson T, Acheson E, Masoli JAH, Knight BA, Hattersley A, Ellard S, Auckland C,
 667 Mahungu TW, Irish-Tavares D, Haque T, Bourgeois Y, Scarlett GP, Partridge DG, Raza
 668 M, Evans C, Johnson K, Liggett S, Baker P, Essex S, Lyons RA, Caller LG, Castellano S,
 669 Williams RJ, Kristiansen M, Roy S, Williams CA, Dyal PL, Tutill HJ, Panchbhaya YN,
 670 Forrest LM, Niola P, Findlay J, Brooks TT, Gavril A, Mestek-Boukhibar L, Weeks S,
 671 Pandey S, Berry Lisa, Jones K, Richter A, Beggs A, Smith CP, Bucca G, Hesketh AR,
 672 Harrison EM, Peacock SJ, Palmer Sophie, Churcher CM, Bellis KL, Girgis ST,
 673 Naydenova P, Blane B, Sridhar S, Ruis C, Forrest S, Cormie C, Gill HK, Dias J,
 674 Higginson EE, Maes M, Young J, Kermack LM, Hadjirin NF, Aggarwal D, Griffith L,
 675 Swinger T, Davidson RK, Rambaut A, Williams T, Balcazar CE, Gallagher MD, O'Toole
 676 Á, Rooke S, Jackson B, Colquhoun R, Ashworth J, Hill V, McCrone J.T., Scher E, Yu X,
 677 Williamson KA, Stanton TD, Michell SL, Bewshea CM, Temperton B, Michelsen ML,
 678 Warwick-Dugdale J, Manley R, Farbos A, Harrison JW, Sambles CM, Studholme DJ,
 679 Jeffries AR, Darby AC, Hiscox JA, Paterson S, Iturriza-Gomara M, Jackson KA, Lucaci
 680 AO, Vamos EE, Hughes M, Rainbow L, Eccles R, Nelson C, Whitehead M, Turtle L,
 681 Haldenby ST, Gregory R, Gemmell M, Kwiatkowski D, Silva TI de, Smith N, Angyal A,
 682 Lindsey BB, Groves DC, Green LR, Wang D, Freeman TM, Parker MD, Keeley AJ,
 683 Parsons PJ, Tucker RM, Brown R, Wyles M, Constantinidou C, Unnikrishnan M, Ott S,
 684 Cheng JKJ, Bridgewater HE, Frost LR, Taylor-Joyce G, Stark R, Baxter L, Alam MT,
 685 Brown PE, McClure PC, Chappell JG, Tsoleridis T, Ball J, Gramatopoulos D, Buck D,
 686 Todd JA, Green A, Trebes A, MacIntyre-Cockett G, Cesare M de, Langford C, Alderton
 687 A, Amato R, Goncalves S, Jackson DK, Johnston I, Sillitoe J, Palmer Steve, Lawniczak
 688 M, Berriman M, Danesh J, Livett R, Shirley L, Farr B, Quail M, Thurston S, Park N,
 689 Betteridge E, Weldon D, Goodwin S, Nelson R, Beaver C, Letchford L, Jackson DA,
 690 Foulser L, McMinn L, Prestwood L, Kay S, Kane L, Dorman MJ, Martincorena I, Puethé
 691 C, Keatley J-P, Tonkin-Hill G, Smith C, Jamroz D, Beale MA, Patel M, Ariani C,
 692 Spencer-Chapman M, Drury E, Lo S, Rajatileka S, Scott C, James K, Buddenborg SK,
 693 Berger DJ, Patel G, Garcia-Casado MV, Dibling T, McGuigan S, Rogers HA, Hunter AD,
 694 Souster E, Neaverson AS, Goodfellow I, Loman NJ, Pybus OG, Robertson DL, Thomson
 695 EC, Rambaut A, Connor TR. 2021a. Evaluating the Effects of SARS-CoV-2 Spike
 696 Mutation D614G on Transmissibility and Pathogenicity. *Cell* **184**:64-75.e11.
 697 doi:10.1016/j.cell.2020.11.020

698 Volz E, Mishra S, Chand M, Barrett JC, Johnson R, Geidelberg L, Hinsley WR, Laydon DJ,
 699 Dabrera G, O'Toole Á, Amato R, Ragonnet-Cronin M, Harrison I, Jackson B, Ariani CV,
 700 Boyd O, Loman NJ, McCrone JT, Gonçalves S, Jorgensen D, Myers R, Hill V, Jackson
 701 DK, Gaythorpe K, Groves N, Sillitoe J, Kwiatkowski DP, consortium TC-19 GU (COG-
 702 U, Flaxman S, Ratmann O, Bhatt S, Hopkins S, Gandy A, Rambaut A, Ferguson NM.
 703 2021b. Transmission of SARS-CoV-2 Lineage B.1.1.7 in England: Insights from linking
 704 epidemiological and genetic data. *Medrxiv* 2020.12.30.20249034.
 705 doi:10.1101/2020.12.30.20249034

706 Wang Z, Schmidt F, Weisblum Y, Muecksch F, Barnes CO, Finkin S, Schaefer-Babajew D,
707 Cipolla M, Gaebler C, Lieberman JA, Oliveira TY, Yang Z, Abernathy ME, Huey-
708 Tubman KE, Hurley A, Turroja M, West KA, Gordon K, Millard KG, Ramos V, Silva JD,
709 Xu J, Colbert RA, Patel R, Dizon J, Unson-O'Brien C, Shimeliovich I, Gazumyan A,
710 Caskey M, Bjorkman PJ, Casellas R, Hatzioannou T, Bieniasz PD, Nussenzweig MC.
711 2021. mRNA vaccine-elicited antibodies to SARS-CoV-2 and circulating variants. *Nature*
712 1–7. doi:10.1038/s41586-021-03324-6

713 Washington NL, Gangavarapu K, Zeller M, Bolze A, Cirulli ET, Barrett KMS, Larsen BB,
714 Anderson C, White S, Cassens T, Jacobs S, Levan G, Nguyen J, Ramirez JM, Rivera-
715 Garcia C, Sandoval E, Wang X, Wong D, Spencer E, Robles-Sikisaka R, Kurzban E,
716 Hughes LD, Deng X, Wang C, Servellita V, Valentine H, Hoff PD, Seaver P, Sathe S,
717 Gietzen K, Sickler B, Antico J, Hoon K, Liu J, Harding A, Bakhtar O, Basler T, Austin B,
718 MacCannell D, Isaksson M, Febbo PG, Becker D, Laurent M, McDonald E, Yeo GW,
719 Knight R, Laurent LC, Feo E de, Worobey M, Chiu CY, Suchard MA, Lu JT, Lee W,
720 Andersen KG. 2021. Emergence and rapid transmission of SARS-CoV-2 B.1.1.7 in the
721 United States. *Cell*. doi:10.1016/j.cell.2021.03.052

722 Wells JA. 1990. Additivity of mutational effects in proteins. *Biochemistry-us* **29**:8509–8517.
723 doi:10.1021/bi00489a001

724 WHO Coronavirus (COVID-19) Dashboard. 2021. <https://covid19.who.int/>

725 Wölfel R, Corman VM, Guggemos W, Seilmaier M, Zange S, Müller MA, Niemeyer D,
726 Jones TC, Vollmar P, Rothe C, Hoelscher M, Bleicker T, Brünink S, Schneider J, Ehmann
727 R, Zwirgmaier K, Drosten C, Wendtner C. 2020. Virological assessment of hospitalized
728 patients with COVID-2019. *Nature* 1–10. doi:10.1038/s41586-020-2196-x

729 Wrapp D, Wang N, Corbett KS, Goldsmith JA, Hsieh C-L, Abiona O, Graham BS, McLellan
730 JS. 2020. Cryo-EM structure of the 2019-nCoV spike in the prefusion conformation.
731 *Science* **367**:1260–1263. doi:10.1126/science.abb2507

732 Yan R, Zhang Y, Li Y, Xia L, Guo Y, Zhou Q. 2020. Structural basis for the recognition of
733 SARS-CoV-2 by full-length human ACE2. *Science* **367**:1444–1448.
734 doi:10.1126/science.abb2762

735 Zahradník J, Marciano S, Shemesh M, Zoler E, Chiaravalli J, Meyer B, Rudich Y, Dym O,
736 Elad N, Schreiber G. 2021. SARS-CoV-2 RBD in vitro evolution follows contagious
737 mutation spread, yet generates an able infection inhibitor. *Biorxiv* 2021.01.06.425392.
738 doi:10.1101/2021.01.06.425392

739 Zhang J, Cai Y, Xiao T, Lu J, Peng H, Sterling SM, Walsh RM, Rits-Volloch S, Zhu H,
740 Woosley AN, Yang W, Sliz P, Chen B. 2021. Structural impact on SARS-CoV-2 spike
741 protein by D614G substitution. *Science* eabf2303. doi:10.1126/science.abf2303

742 Zhang L, Jackson CB, Mou H, Ojha A, Peng H, Quinlan BD, Rangarajan ES, Pan A,
743 Vanderheiden A, Suthar MS, Li W, Iizard T, Rader C, Farzan M, Choe H. 2020. SARS-
744 CoV-2 spike-protein D614G mutation increases virion spike density and infectivity. *Nat*
745 *Commun* **11**:6013. doi:10.1038/s41467-020-19808-4

746 Zhou D, Dejnirattisai W, Supasa P, Liu C, Mentzer AJ, Ginn HM, Zhao Y, Duyvesteyn
747 HME, Tuekprakhon A, Nutalai R, Wang B, Paesen GC, Lopez-Camacho C, Slon-Campos
748 J, Hallis B, Coombes N, Bewley K, Charlton S, Walter TS, Skelly D, Lumley SF, Dold C,
749 Levin R, Dong T, Pollard AJ, Knight JC, Crook D, Lambe T, Clutterbuck E, Bibi S,
750 Flaxman A, Bittaye M, Belij-Rammerstorfer S, Gilbert S, James W, Carroll MW,
751 Klenerman P, Barnes E, Dunachie SJ, Fry EE, Mongkolspaya J, Ren J, Stuart DI, Srean
752 GR. 2021. Evidence of escape of SARS-CoV-2 variant B.1.351 from natural and vaccine
753 induced sera. *Cell*. doi:10.1016/j.cell.2021.02.037

754 Zhou H, Dcosta BM, Samanovic MI, Mulligan MJ, Landau NR, Tada T. 2021. B.1.526
755 SARS-CoV-2 variants identified in New York City are neutralized by vaccine-elicited and
756 therapeutic monoclonal antibodies. *Biorxiv* 2021.03.24.436620.
757 doi:10.1101/2021.03.24.436620

758

Table 1. Affinity and kinetic data for RBD variants and ACE2 variants

Mean and SD of the k_{off} , k_{on} , calculated K_D , and equilibrium K_D values for all RBD variants binding all ACE2 variants. For most measurements $n = 3$; the exceptions were RBD WT/ACE2 WT equilibrium K_D measurements ($n = 24$) and other RBD WT measurements ($n = 6$). UK2 refers to the VOC-202102-02 variant.

	k_{off} (s^{-1})	SD	k_{on} ($\mu\text{M}^{-1}\text{s}^{-1}$)	SD	K_D Calc. (nM)	SD	K_D Equi. (nM)	SD
RBD over WT ACE2								
WT	0.0668	0.00113	0.90	0.05	74.4	4.0	62.6	7.7
K417N	0.177	0.00416	0.49	0.05	364	29	349	10
K417T	0.126	0.00510	0.55	0.04	230	23	226	19
S477N	0.0348	0.00037	0.81	0.03	42.9	2.1	42.6	3.0
E484K	0.0818	0.00183	1.54	0.03	53.1	1.7	52.6	2.0
N501Y (Alpha)	0.0111	0.00017	1.59	0.04	7.0	0.25	5.5	2.4
K417N/E484K	0.251	0.00799	1.02	0.07	247	23	251	23
K417T/E484K	0.168	0.00573	1.10	0.05	153	12	147	8.6
E484K/N501Y (UK2)	0.0118	0.00037	2.33	0.10	5.1	0.36	3.7	2.7
K417N/E484K/N501Y (Beta)	0.0291	0.00076	1.46	0.06	20.0	0.70	17.4	3.1
K417T/E484K/N501Y (Gamma)	0.0211	0.00021	1.56	0.07	13.5	0.45	12.2	3.4
RBD over S19P ACE2								
WT	0.0298	0.00039	1.50	0.12	20.0	1.3	30.5	2.2
K417N	0.0782	0.00284	0.72	0.04	108	2.8	129	8.2
K417T	0.0521	0.00196	0.69	0.02	75.8	4.7	87.8	7.0
S477N	0.0257	0.00016	1.05	0.07	24.6	1.7	30.3	2.7
E484K	0.0325	0.00031	2.02	0.08	16.2	0.55	20.8	1.3
N501Y (Alpha)	0.0051	0.00004	2.31	0.09	2.2	0.09	3.5	0.4
K417N/E484K	0.0961	0.00198	1.28	0.11	75.6	7.1	91.3	6.5
K417T/E484K	0.0660	0.00255	1.45	0.03	45.5	2.5	53.8	1.5
E484K/N501Y (UK2)	0.0051	0.00008	3.10	0.10	1.7	0.05	3.4	0.4
K417N/E484K/N501Y (Beta)	0.0122	0.00009	2.16	0.03	5.7	0.07	10.4	1.2
K417T/E484K/N501Y (Gamma)	0.0085	0.00007	2.11	0.05	4.0	0.07	6.1	1.3
RBD over K26R ACE2								
S477N	0.0240	0.00009	1.07	0.05	22.6	1.1	33.4	1.3
WT	0.0500	0.00062	1.60	0.16	31.4	2.6	48.8	2.5
K417N	0.154	0.00789	0.88	0.07	175	8.1	237	15
K417T	0.101	0.00079	0.81	0.12	127	17.4	154	2.8
S477N	0.0240	0.00009	1.07	0.05	22.6	1.1	33.4	1.3
E484K	0.0587	0.00109	2.03	0.03	28.9	1.0	35.9	1.5
N501Y (Alpha)	0.0081	0.00002	2.34	0.09	3.5	0.15	7.5	1.5
K417N/E484K	0.191	0.00481	1.48	0.15	130	9.4	166	11
K417T/E484K	0.135	0.00407	1.53	0.02	88.0	3.9	105	0.7
E484K/N501Y (UK2)	0.0085	0.00018	3.06	0.23	2.8	0.17	6.4	0.3
K417N/E484K/N501Y (Beta)	0.0234	0.00040	2.13	0.05	11.0	0.28	18.7	2.0
K417T/E484K/N501Y (Gamma)	0.0164	0.00028	2.21	0.06	7.4	0.33	15.3	0.8

Table 2. $\Delta\Delta G$ for RBD variants binding to ACE2 variants

Mean and SD of $\Delta\Delta G$ ($n = 3$, kcal/mol) were determined as described in the Materials and Methods using the calculated K_D values in Table 1. UK2 refers to the VOC-202102-02 variant.

	ACE2 WT		ACE2 S19P		ACE2 K26R	
RBD variant	$\Delta\Delta G$	SD	$\Delta\Delta G$	SD	$\Delta\Delta G$	SD
WT	0.00	0.00	0.79	0.05	0.52	0.06
K417N	-0.96	0.06	-0.23	0.04	-0.52	0.04
K417T	-0.68	0.07	-0.01	0.05	-0.32	0.09
S477N	0.33	0.04	0.67	0.05	0.72	0.04
E484K	0.20	0.04	0.92	0.04	0.57	0.04
N501Y (Alpha)	1.43	0.04	2.13	0.04	1.86	0.04
K417N/E484K	-0.72	0.07	-0.01	0.07	-0.34	0.06
K417T/E484K	-0.43	0.06	0.30	0.05	-0.10	0.04
E484K/N501Y (UK2)	1.62	0.05	2.30	0.04	1.98	0.05
K417N/E484K/N501Y (Beta)	0.79	0.04	1.56	0.03	1.16	0.04
K417T/E484K/N501Y (Gamma)	1.03	0.04	1.76	0.03	1.39	0.04

Figure Legends

Figure 1. Spike RBD and ACE2 variants analysed in this study.

(A) Phylogenetic tree illustrating the clades containing the RBD mutations investigated in this study. Constructed using TreeTime (Sagulenko et al., 2018) from the Nextstrain Global (Hadfield et al., 2018) sample of SARS-CoV-2 sequences from the GISAID database (Shu and McCauley, 2017) (Accessed 15th April 2021, N = 4,017). (B) Alignment illustrating the Spike residues that differ between SARS-CoV-2 variants, with the RBD mutants boxed. The variants are labelled with their clade designation from Nextstrain (Hadfield et al., 2018) and/or PANGO lineage (Rambaut et al., 2020), where relevant. The RBD mutations were collated from CoVariants (Hodcroft, 2021) and Nextstrain. (C) The structure of human ACE2 (green) in complex with SARS-CoV-2 Spike RBD (cyan). The area enclosed by the box is shown enlarged on the right, with the residues mutated in this study labelled. Drawn using UCSF Chimera (Pettersen et al., 2004) using coordinates from PDB 6m0j (Lan et al., 2020).

Figure 1-figure supplement 1. Emergence of the same RBD mutations in multiple SAR2-CoV-2 clades.

The figure highlights the SARS-CoV-2 clades containing RBD mutations investigated in this study. The phylogenetic trees were constructed as in Figure 1A from SARS-CoV-2 sequences accessed on the 22nd April 2021 (N = 3,914). (A) N501Y has emerged independently in the three clades 501Y.V1, 501Y.V2, and 501Y.V3. Mutation to T at this position has also occurred frequently. (B) E484K has also been observed independently of its main progenitor clades 501Y.V2 and 501Y.V3. E484Q and E484G have also been observed. (C) S477N has been observed beyond clades 20F and 20A.EU2. Mutations to I and R have also been occasionally observed at this position. (D) Mutations of K417 to N and T have been observed almost exclusively in the 20H.501Y.V2 and 20J.501Y.V3 clades.

Figure 2. SPR analysis

(A) Overlay of traces showing association and dissociation when WT RBD is injected for 30 s at the indicated concentration over immobilized WT ACE2. The right panel shows an expanded view of the dissociation phase. The blue lines show the fits used for determining the k_{on} and k_{off} . The k_{on} was determined as described in Figure 2-figure supplement 2. The k_{off} (B) and k_{on} (C) values measured at different levels of immobilized ACE2 are shown. (D) The equilibrium K_D was determined by plotting the binding at equilibrium against [RBD] injected. Data from experiment shown in A. (E) The equilibrium K_D measured at different levels of immobilized ACE2 are shown.

Figure 2-figure supplement 1. Protein purification. Size-exclusion chromatography traces of the indicated ACE2 and RBD proteins and reducing SDS-PAGE of the indicated peak fractions. UK2 refers to the VOC-202102-02 variants. In preparations of RBD, unidentified ~60 kDa contaminants were present at various levels, but always < 5% by densitometry.

Figure 2-figure supplement 2. Determining the k_{on} and k_{off} . Analysis of data from the fits in Figure 2A. (A) A plot of k_{off} obtained for each injection versus [RBD]. (B) A plot of k_{obs} for each injection versus [RBD]. The line shows a constrained fit of the equation $k_{obs} = k_{on} * [RBD] + k_{off}$, using the k_{off} obtained in (A). The k_{on} was obtained from the slope.

Figure 3. Effect of RBD mutations on binding to WT ACE2

Overlay of traces showing association and dissociation of N501Y (A) and K417N (B) RBD variants when injected at a range of concentrations over immobilised WT ACE2. The right panels show an expanded view of the dissociation phase. The blue lines show fits used for determining the k_{on} and k_{off} . (C) The fold change relative to WT RBD of the calculated K_D , k_{on} , and k_{off} for binding of the indicated RBD variants to immobilised WT ACE2 (error bars show SD, $n = 3$). Representative sensorgrams from all mutants shown in Figure 3-figure supplement 2, and the mean values from multiple repeats are in Table 1. (D) The blue lines show the measured $\Delta\Delta G$ for indicated RBD variants. The red lines show the predicted $\Delta\Delta G$ for the RBD variants with multiple mutations, which were calculated by adding $\Delta\Delta G$ values for single mutation variants (error bars show SD, $n = 3$).

Figure 3-figure supplement 1. Mass transport controls for RBD. The k_{off} (A) and k_{on} (B) for E484K/N501Y (UK2) RBD binding WT ACE2 at a range of surface immobilisations ($n = 12$). UK2 refers to VOC-202102-02.

Figure 3-figure supplement 2. Representative SPR data for RBD variants binding to WT ACE2. Binding traces for the indicated RBD variants injected at different concentrations over immobilised WT ACE2. The right panels show an expanded view of the dissociation phase. The blue lines show fits used for determining the k_{on} and k_{off} . UK2 refers to the VOC-202102-02 variant.

Figure 4. Effect of mutations in ACE2

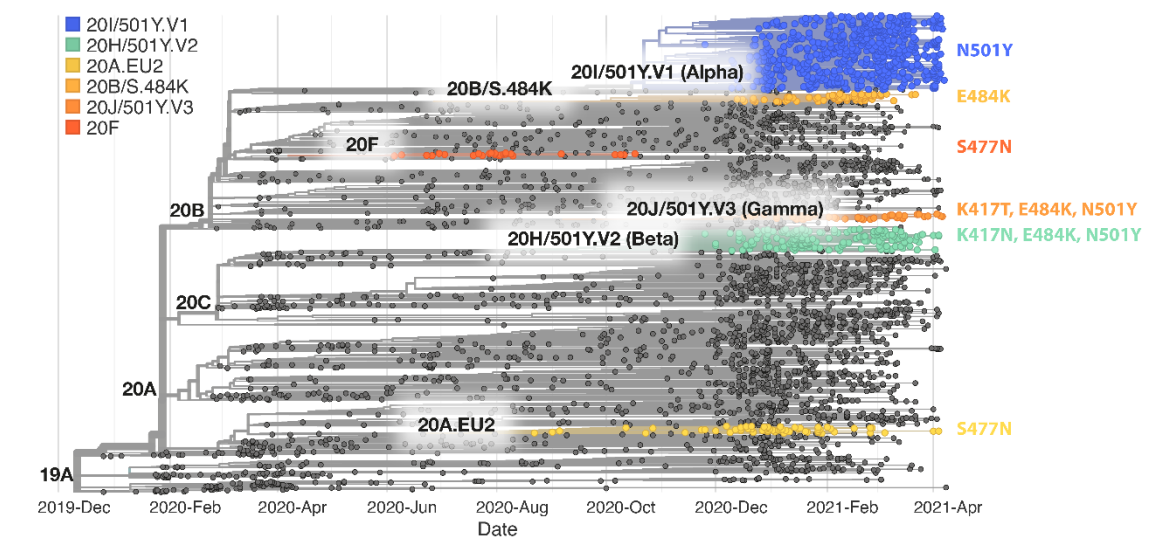
(A) The fold change relative to WT ACE2 of the calculated K_D , k_{on} , and k_{off} for the interaction of WT RBD and the indicated ACE2 variants (Error bars show SD, $n = 3$). (B, C) Show the difference ($\Delta\Delta\Delta G$) between the measured and predicted $\Delta\Delta G$ for S19P (B) and K26R (C) ACE2 variants binding to the indicated RBD variants, calculated from data in Table 2. The predicted $\Delta\Delta G$ values for each variant RBD/variant ACE2 interaction were calculated from the sum of the $\Delta\Delta G$ for the ACE2 variant binding WT RBD and the $\Delta\Delta G$ for the RBD variant binding WT ACE2 (Table 2).

Figure 4-figure supplement 1. Representative SPR data for WT RBD binding ACE2 variants

Binding traces for the WT RBD injected at different concentrations over the indicated immobilized ACE2 variants. The right panels show an expanded view of the dissociation phase. The blue lines show fits used for determining the k_{on} and k_{off} .

Figure 1

A



B

	RBD																																			
19A (Ref.)	5	13	18	20	26	52	67	69	70	80	95	138	144	190	215	241	242	243	253	417	477	484	501	570	614	655	677	681	701	716	888	982	1118	1027	1176	
20I/501Y.V1 (B.1.1.7; Alpha)	L	S	L	T	P	Q	A	H	V	D	T	D	Y	R	D	L	L	A	D	K	S	E	N	A	D	H	Q	P	A	T	F	S	D	T	V	
20H/501Y.V2 (B.1.351; Beta)	.	.	F	A	G	N	.	K	Y	D	G	.	.	H	.	I	.	A	H	.	.	
20J/501Y.V3 (P.1; Gamma)	.	.	F	N	S	A	.	Y	.	S	T	.	K	Y	.	G	Y	.	.	V	I	F	
20B/S.484K (P.2; Zeta)	R	V	K	.	.	.	G	F
20A/S.484K (B.1.525; Eta)	K	.	.	.	G	.	H	.	.	L	
20C/S.484K (B.1.526; Iota)	F	I	G	.	K	.	.	G	.	.	.	V	
20A.EU2	N	.	.	.	G	
20F	N	.	.	.	G	

C

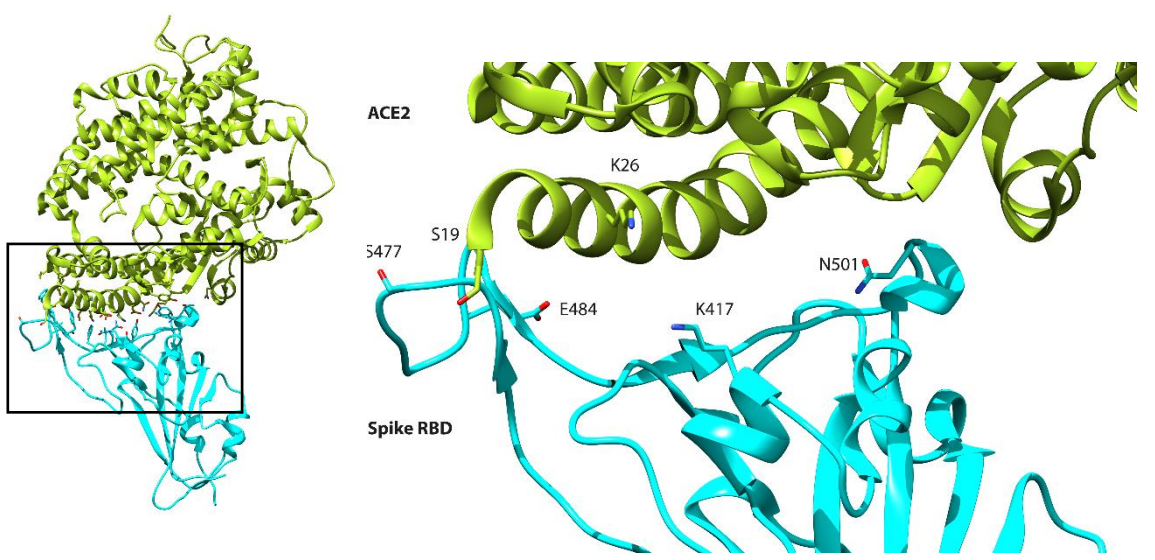


Figure 1–figure supplement 1

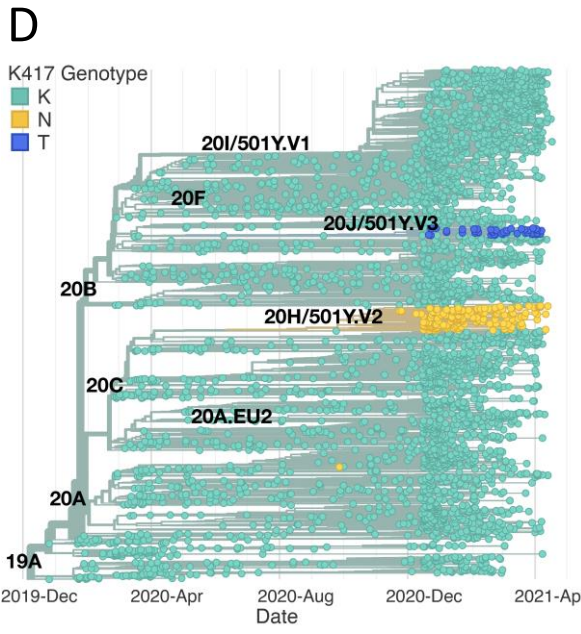
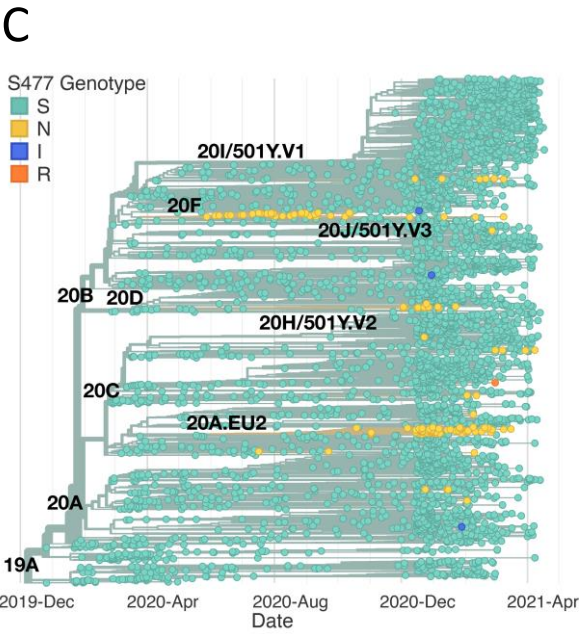
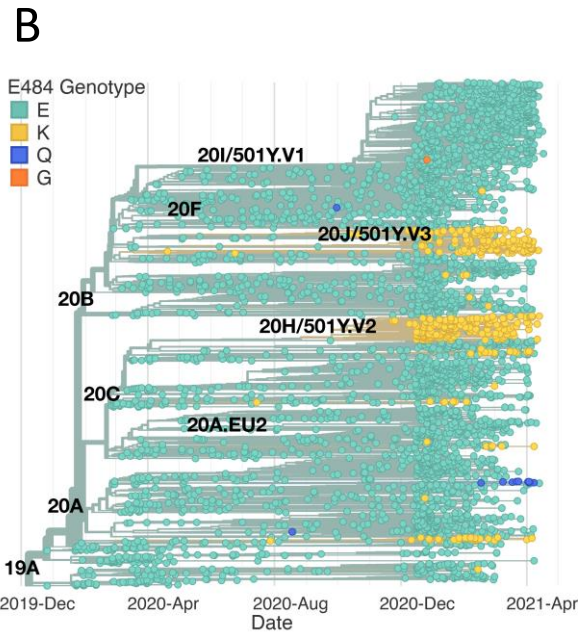
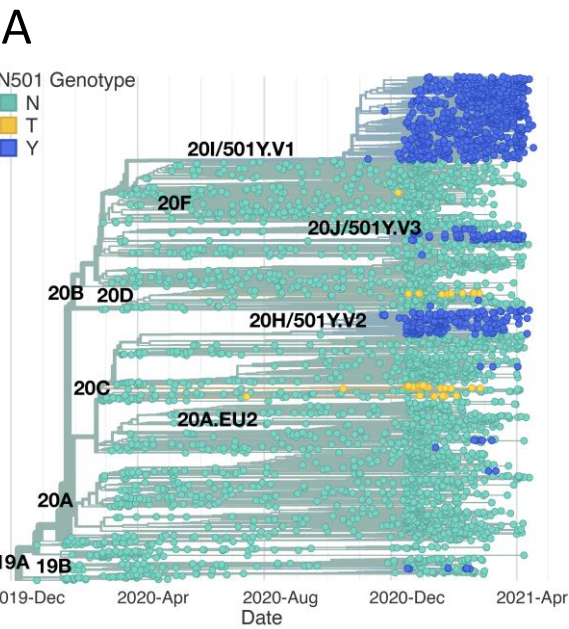
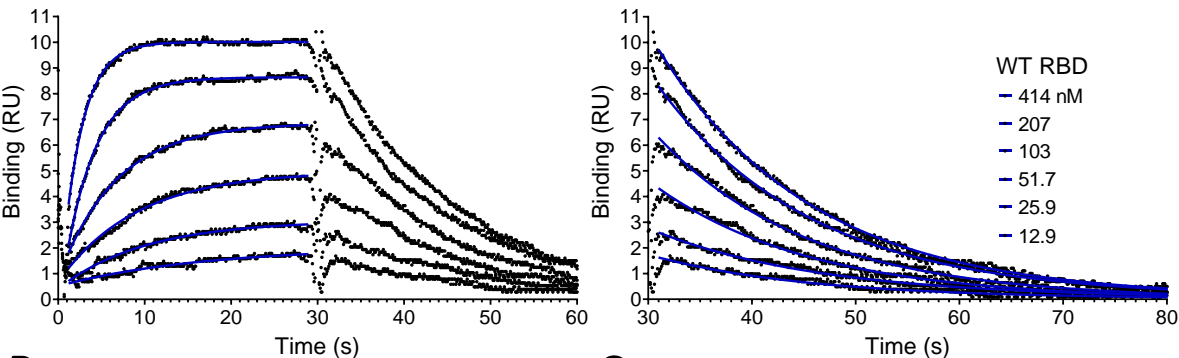
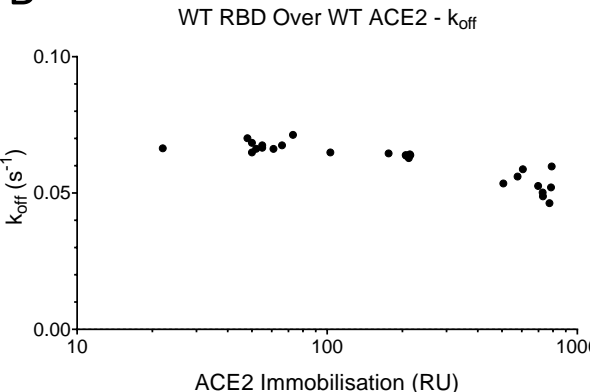


Figure 2

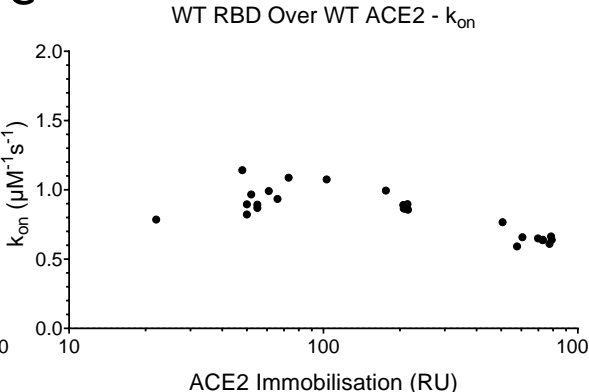
A



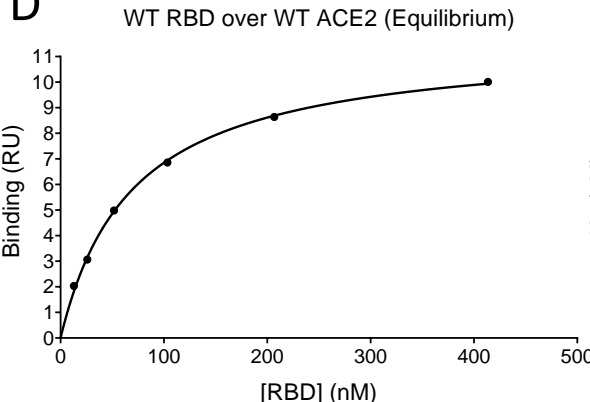
B



C



D



E

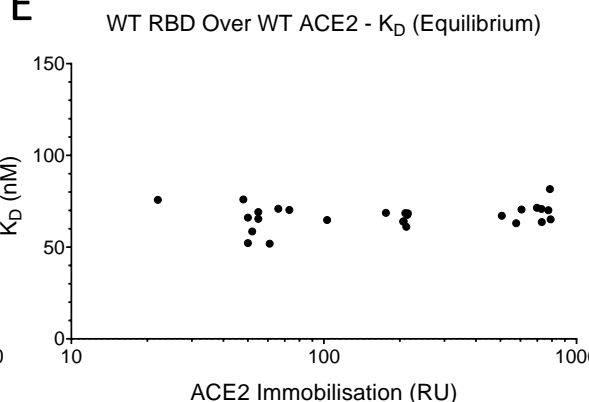


Figure 2-figure supplement 1

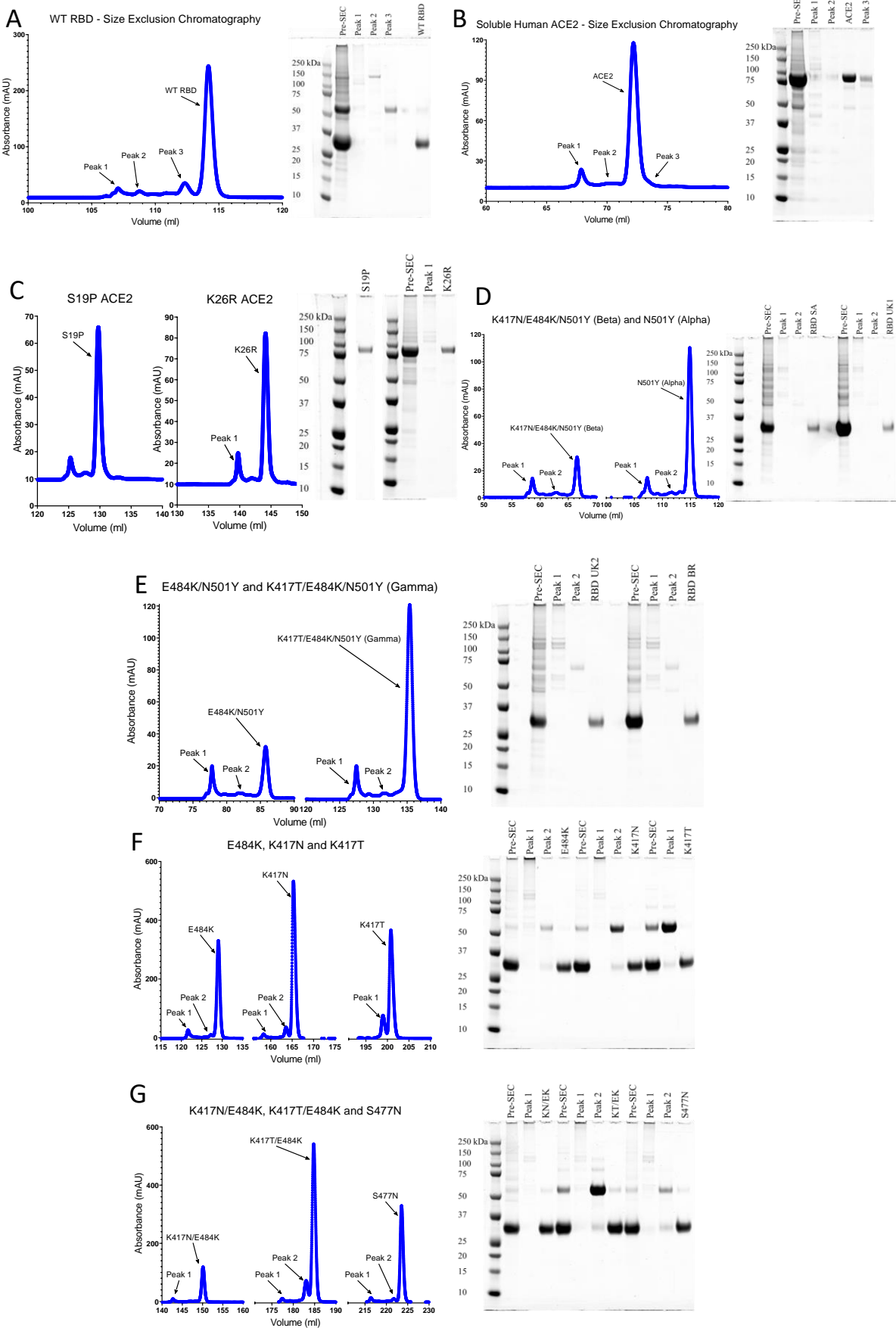
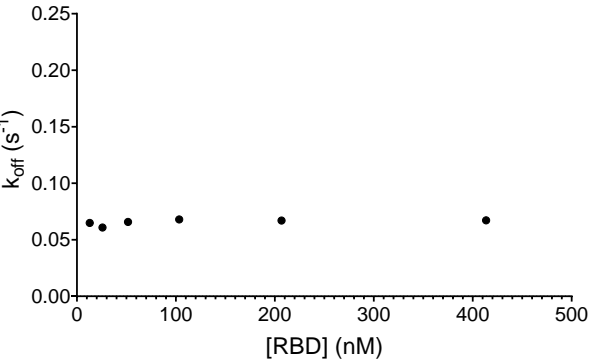


Figure 2-figure supplement 2

A



B

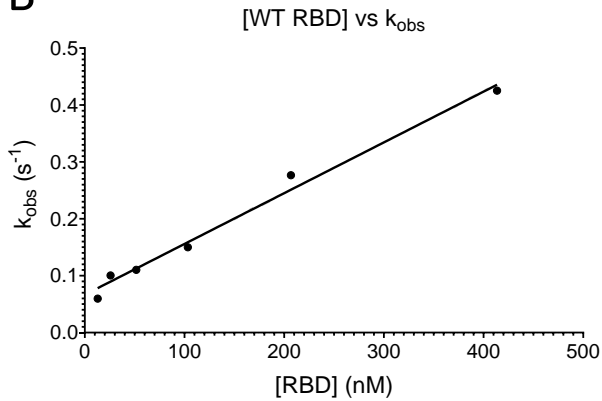
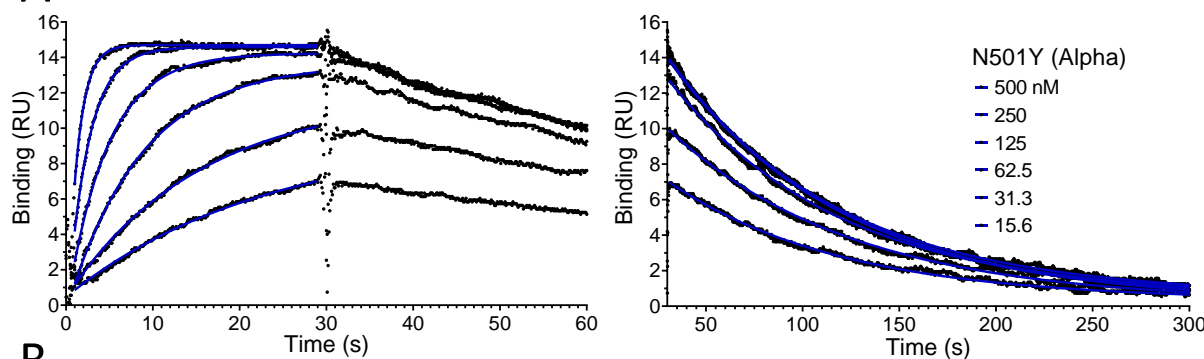
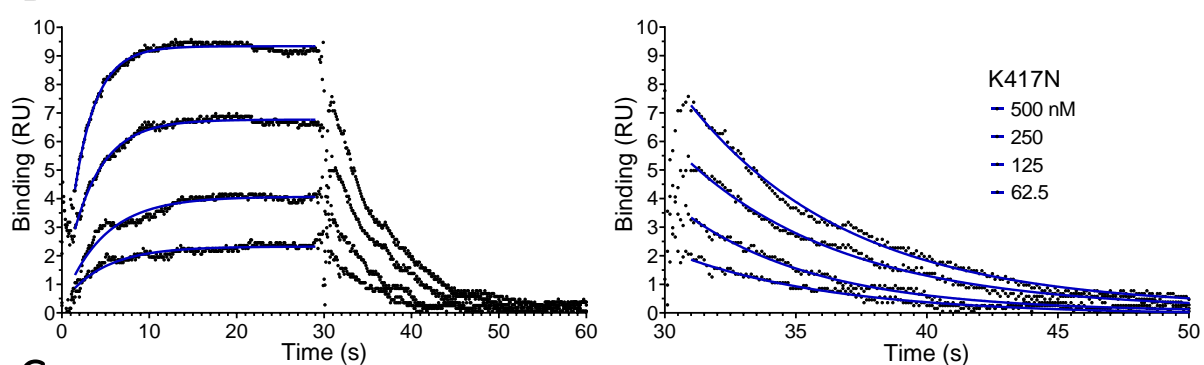


Figure 3

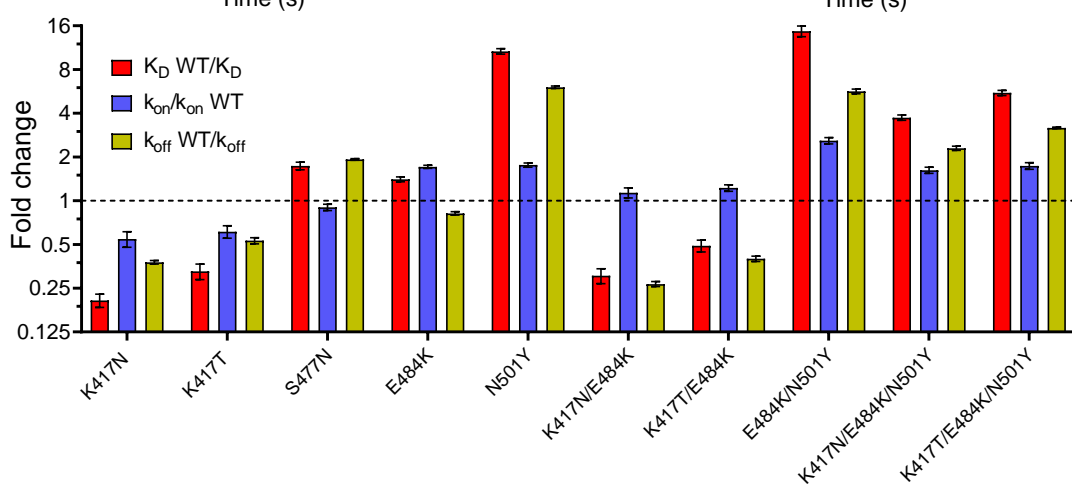
A



B



C



D

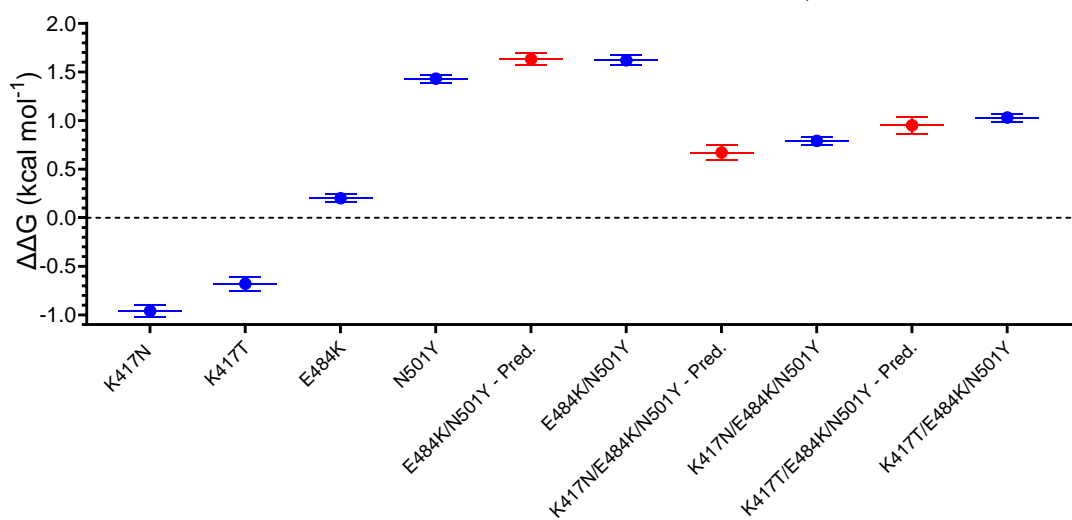
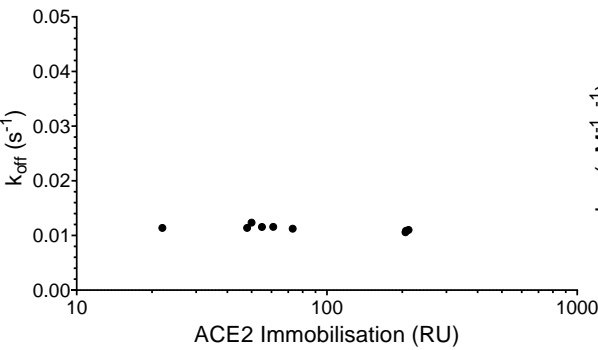


Figure 3-figure supplement 1

A

E484K/N501Y (UK2) Over WT ACE2 - k_{off}



B

E484K/N501Y (UK2) Over WT ACE2 - k_{on}

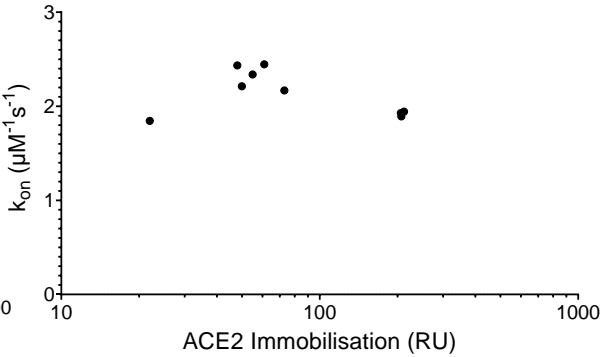


Figure 3-figure supplement 2

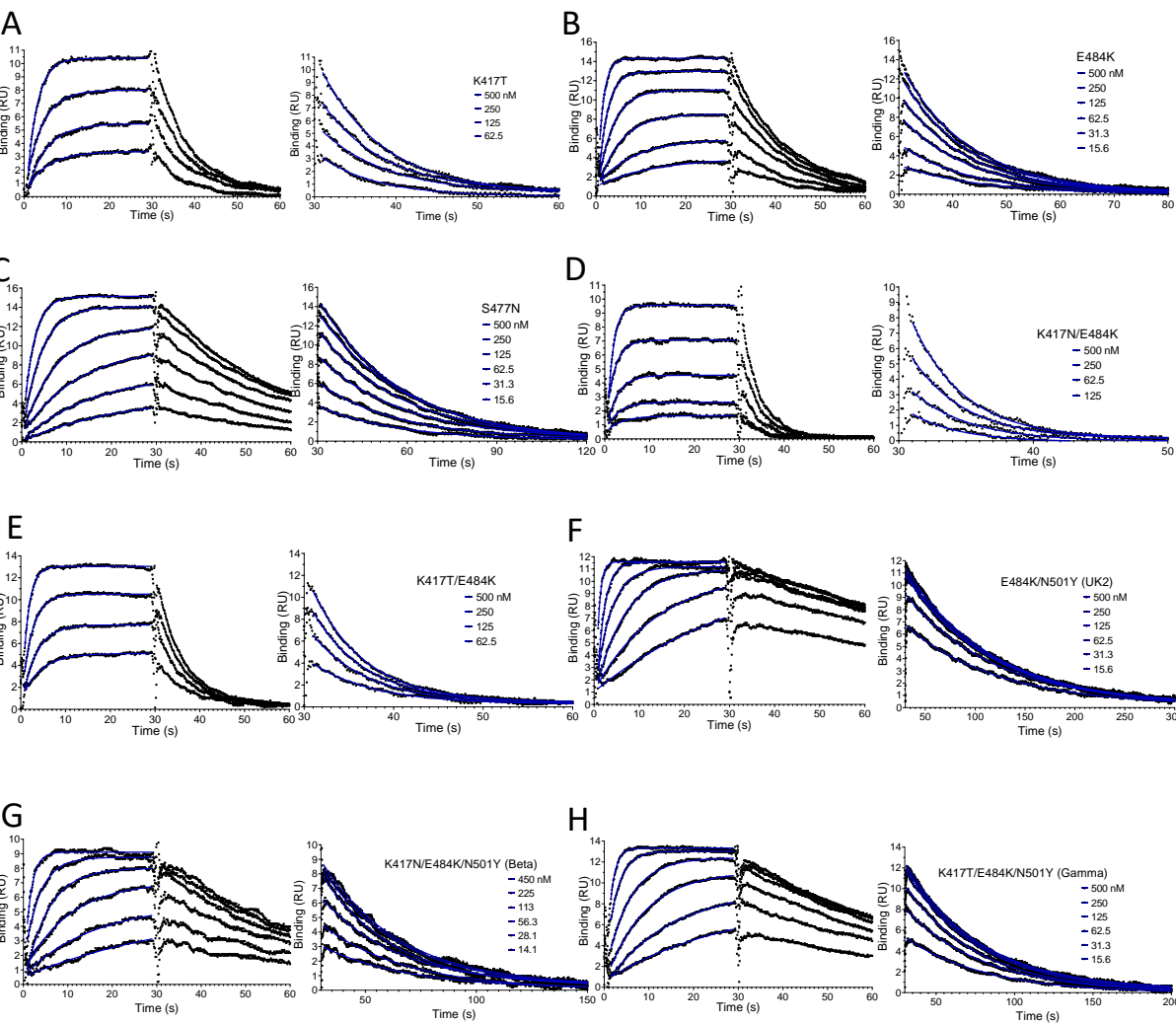


Figure 4

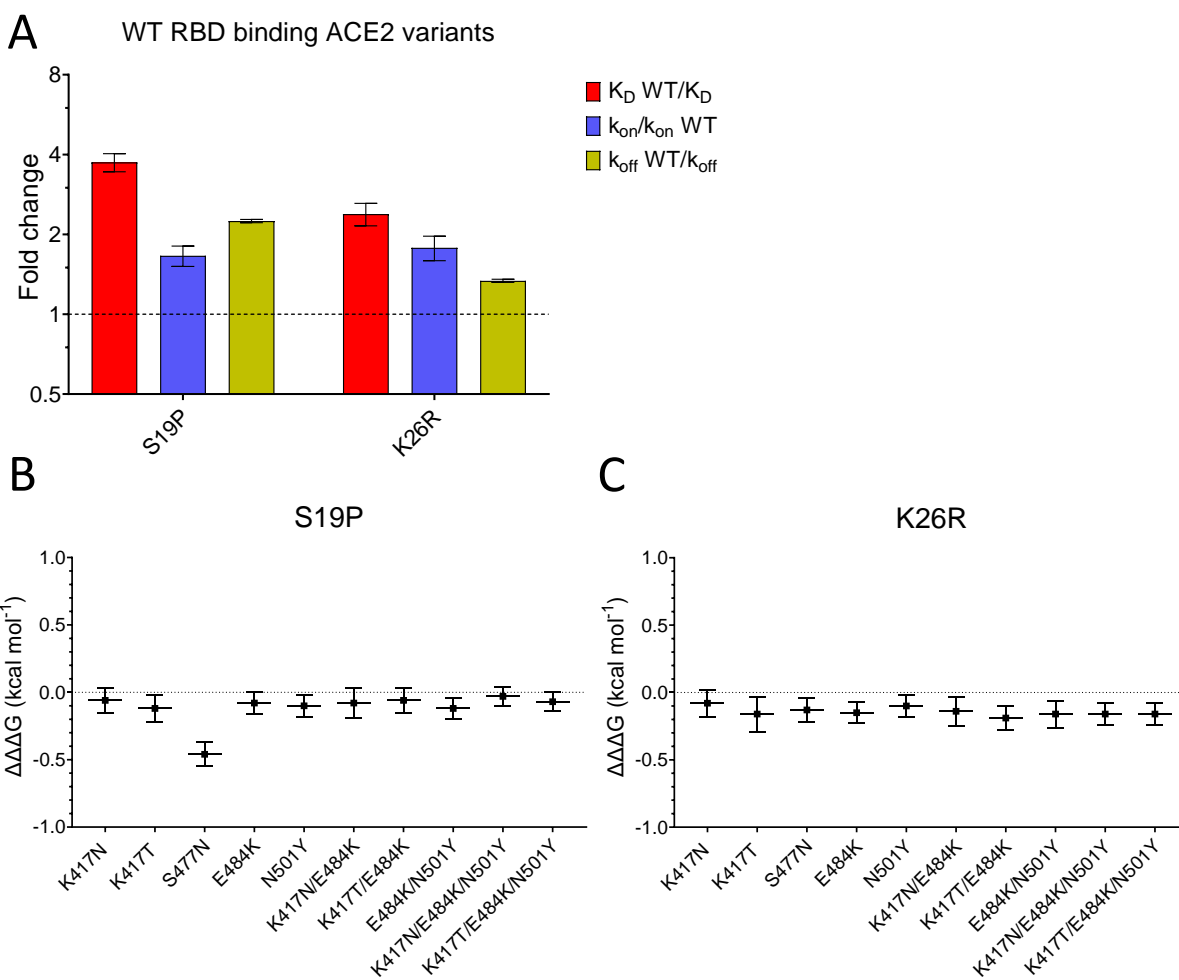
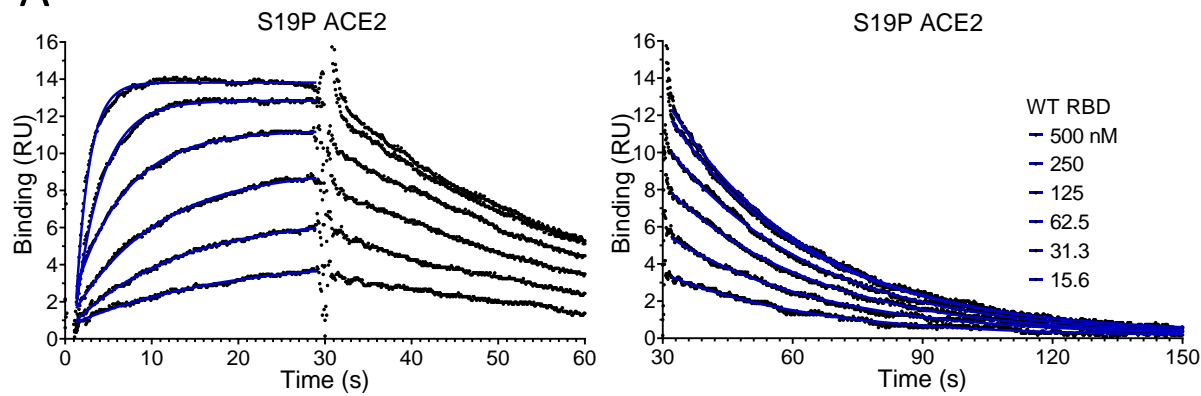


Figure 4-figure supplement 1

A



B

